

Kinetics of the OH + NO₂ reaction: Effect of water vapour and new parameterisation for global modelling.

Damien Amedro¹, Matias Berasategui¹, Arne J. C. Bunkan¹, Andrea Pozzer¹, Jos Lelieveld¹ and John N. Crowley¹

5 ¹Division of Atmospheric Chemistry, Max-Planck-Institute for Chemistry, 55128 Mainz, Germany

Correspondence to: John N. Crowley (john.crowley@mpic.de)

Abstract. The effect of water vapour on the rate coefficient for the atmospherically important, termolecular reaction between OH and NO₂ was determined in He-H₂O (277, 291 and 332 K) and N₂-H₂O bath gases (292 K). Combining pulsed laser photolytic generation of OH and its detection by laser induced fluorescence (PLP-LIF) with in-situ, optical measurement of both NO₂ and H₂O we were able to show that (in contrast to previous investigations) the presence of H₂O increases the rate coefficient significantly. We derive a rate coefficient for H₂O bath gas at the low-pressure limit ($k_0^{\text{H}_2\text{O}}$) of $15.9 \times 10^{-30} \text{ cm}^6 \text{ molecule}^{-2} \text{ s}^{-1}$. This indicates that H₂O is a more efficient collisional quencher (by a factor of ≈ 6) of the initially formed HO-NO₂ association complex than N₂ and a factor ≈ 8 more efficient than O₂. Ignoring the effect of water-vapour will lead to an underestimation of the rate coefficient by up to 15% e.g. in the tropical boundary layer. Combining the new experimental results from this study with those from the companion paper in which we report rate coefficients obtained in N₂ and O₂ bath gases (Amedro et al., 2019) we derive a new parameterisation for atmospheric modelling of the OH + NO₂ reaction and use this in a chemical transport model (EMAC) to examine the impact of the new data on the global distribution of NO₂, HNO₃ and OH. Use of the new parameters (rather than those given in the IUPAC and NASA evaluations) result in significant changes in the HNO₃ / NO₂ ratio and NO_x concentrations, the sign of which depends on which evaluation is used as reference. The model predicts the presence of HOONO (formed along with HNO₃ in the title reaction) in concentrations similar to those of HO₂NO₂ at the tropical tropopause.

1 Introduction

In our recent study of the title reaction (Amedro et al., 2019), we reported extensive measurements of the rate constant (k_1) for the termolecular reaction between OH and NO₂ (R1) in N₂ and O₂ bath gas over a large range of temperature and pressures.



Reaction (R1) converts NO₂ to nitric acid (HNO₃) and peroxyxynitrous acid (HOONO), and its rate strongly influences the relative abundance of atmospheric NO_x (NO₂ + NO) and longer-lived “reservoirs” of NO_x which include e.g. HNO₃ and organic nitrates. It also converts OH (the main initiator of atmospheric oxidation) to a long-lived reservoir, HNO₃. As the abundance of OH and NO_x directly impact on photochemical ozone formation and the lifetimes of greenhouse gases, reaction (R1) may be considered one of the most important gas-phase processes in atmospheric science (Newsome and Evans, 2017). As outlined by Amedro et al. (2019), the rate coefficients and product-branching for this reaction are dependent on pressure and temperature and also on the bath-gas identity, i.e. the identity of the collision partner, M in reaction (R1). The per collision efficiency of energy transfer from the initially “hot” association complex to bath gas can vary considerably, with more complex bath gases possessing more degrees of freedom and bonds with similar vibrational frequencies to those in the association complex being generally more efficient. In this sense, we may expect H₂O to be better than N₂ or O₂ in quenching [HO-NO₂][#]. In this second part of our study of the reaction between OH and NO₂, we extend the experiments to H₂O and He bath-gases. After N₂ ($\approx 78\%$) and O₂ ($\approx 21\%$) water vapour is the third most abundant gaseous species in the lower atmosphere. Its

concentration is highly variable in time and space, varying in mixing ratio from a few percent at sea level to parts-per-million in the stratosphere. Most of the atmosphere's water vapour is present in the planetary boundary layer where its average mixing ratio on the global scale is $\approx 1\%$ but which may exceed 5% in tropical regions.

The effect of water vapour on gas-phase radical-reactions has been the subject of numerous studies (Buszek et al., 2011) and is sometimes interpreted in terms of formation of H₂O-radical complexes leading, via a chaperone type mechanism, to an increase in the rate constant. An important example of this is the HO₂ self-reaction for which the rate constant increases by a factor of up to two in the presence of water vapour due to formation of an HO₂-H₂O complex (Lii et al., 1981; Kircher and Sander, 1984). Theoretical calculations (Allodi et al., 2006; Sadanaga et al., 2006; Thomsen et al., 2012) suggest that, under our experimental conditions, the fraction of OH and NO₂ clustered with H₂O is $< 0.1\%$ which is insufficient to significantly impact on k_1 .

On the other hand, the role of H₂O as a collision partner in termolecular, atmospheric reactions has rarely been reported though its potential impact has been highlighted (Trope, 2003). Indeed, water vapour is known to be a more efficient third-body collider, by up to an order of magnitude compared to N₂ in termolecular reactions such as H + H + M, H + OH + M and H + O₂ + M (Getzinger and Blair, 1969; Michael et al., 2002; Fernandes et al., 2008; Shao et al., 2019).

The conclusions of three previous experiments examining the role of H₂O in kinetic studies of reaction (R1) are highly divergent, with the addition of H₂O found to 1) increase the rate coefficient (Simonaitis and Heicklen, 1972), 2) have no measureable effect (D'Ottone et al., 2001) or 3) even reduce it (Sadanaga et al., 2006). The overall aim of this research was to clarify these differences and provide quantitative data on the third-body efficiency of H₂O for the title reaction. Based on the kinetic data for the water vapour effect reported in this manuscript and in N₂ and O₂ presented in the first part of this study (Amedro et al., 2019) we have generated a new parameterisation for the overall rate coefficient, k_1 , and examined its impact on atmospheric OH, NO_x and NO_y in a global chemical transport model.

2. Experimental details

The details of the experimental set-up have been published previously (Wollenhaupt et al., 2000; Amedro et al., 2019) and only a brief description is given here.

2.1 PLP-LIF technique

The experiments were carried out in a quartz reactor of volume 500 cm³ which was thermostatted to the desired temperature by circulating a 60:40 mixture of ethylene glycol-water. The pressure in the reactor was monitored with 100 and 1000 Torr capacitance manometers. Flow rates were chosen so that a fresh gas sample was available for photolysis at each laser pulse (laser frequency, 10 Hz), thus preventing build-up of products. Pulses of 248 nm laser light (≈ 20 ns) for OH generation from HNO₃, H₂O₂ and O₃/H₂O precursors were provided by an excimer laser (Compex 205 F, Coherent) operated using KrF.



OH concentrations ($10^{11} - 10^{12}$ molecule cm⁻³) were similar to those reported by Amedro et al. (2019) and the same arguments, which rule out significant influence of secondary reactions, apply. The concentration ranges of the H₂O₂, HNO₃ and O₃ precursors are listed in the notes to Tables 1 and 2.

OH was detected following excitation of the OH $A^2\Sigma(v'=1) \leftarrow X^2\Pi(v''=0)$ transition (Q11(1) at 281.997 nm using a YAG-pumped dye laser (Quantel-Brilliant B and Lambda-Physik Scanmate). OH fluorescence was detected by a photomultiplier tube (PMT) screened by a 309 nm interference filter and a BG 26 glass cut-off filter.

2.2 On-line absorption measurement of NO₂ and H₂O concentration

80 As discussed by Amedro et al. (2019), the determination of the NO₂ concentration is critical for accurate measurement of k_1 . We therefore deployed in-situ, broad-band (405 – 440 nm) and single wavelength (365 nm) optical absorption spectroscopy. The former was located prior (in flow) to the quartz-reactor, the latter was located behind the quartz-reactor. Using the broadband cell, the NO₂ concentration was retrieved by least square fitting from 405 to 440 nm to a reference spectrum (Vandaele et al., 2002) degraded to the resolution of our spectrometer. Simultaneously, we measured NO₂ at 365 nm using the
85 absorption cross-section $5.89 \times 10^{-19} \text{ cm}^2 \text{ molecule}^{-1}$ determined previously by Amedro et al. (2019) who give a detailed description of the NO₂ concentration measurements and the choice of reference spectrum. For the temperatures used in this study, corrections to the NO₂ concentration due to formation of the N₂O₄ dimer were not necessary. For the present experiments, a third absorption cell ($l = 40 \text{ cm}$) was placed downstream of the quartz-reactor to measure the H₂O concentration at 184.95 nm. This set-up used a low-pressure Hg-Penray lamp isolated with a 185 nm interference filter
90 as light source. Optical extinction was converted to concentrations using a cross-section of $7.14 \times 10^{-20} \text{ cm}^2 \text{ molecule}^{-1}$ (Cantrell et al., 1997).

2.3 Chemicals

N₂ and He (Westfalen 99.999%) were used without further purification. H₂O₂ (AppliChem, 50 wt. %) was concentrated to >90 wt.% by vacuum distillation. Anhydrous nitric acid was prepared by mixing KNO₃ (Sigma Aldrich, 99%) and H₂SO₄ (Roth,
95 98%), and condensing HNO₃ vapour into a liquid nitrogen trap. NO (3.5 AirLiquide) was purified of other nitrogen oxides by fractional, vacuum distillation and then converted to NO₂ via reaction with a large excess of O₂. The NO₂ thus made was trapped in liquid N₂ and the excess O₂ was pumped out. The resulting NO₂ was stored as a mixture of ~0.5% NO₂ in N₂ or ~5.5% NO₂ in He. Distilled H₂O (Merck, Liquid Chromatography grade) was degassed before use and kept at constant temperature.

100 3 Results and Discussion

3.1 Measurements of k_1 in He bath-gas and comparison with literature

Our study of the role of H₂O as collision partner in reaction (R1) was carried out in mixtures of He-H₂O and N₂-H₂O. In order to separate the effects of H₂O and He, we also required accurate rate coefficients for pure He bath gas, which we describe below. As for the N₂ and O₂ bath-gas datasets (Amedro et al., 2019), the experiments were carried out under pseudo-first-order
105 conditions ($[\text{NO}_2] \gg [\text{OH}]$) so that Eqn. 1-2 describe the decay of OH and the derivation of the bimolecular rate coefficient, k_1 .

$$[\text{OH}]_t = [\text{OH}]_0 \exp(-k' t) \quad (1)$$

where $[\text{OH}]_t$ is the concentration (molecule cm⁻³) at time t after the laser pulse. k' is the pseudo-first order rate coefficient and is defined as

$$110 \quad k' = k_1[\text{NO}_2] + k_d \quad (2)$$

where k_d (s⁻¹) accounts for OH-loss due to diffusion out of the reaction zone and reaction with its photolytic precursors such as HNO₃ or H₂O₂.

An exemplary dataset illustrating OH decays and a plot of k' versus $[\text{NO}_2]$ is given in Fig. S1 of the supplementary information).

115 Values of k_1 obtained in He bath-gas (25-690 Torr, 292 K) are summarised in Fig. 1 and 2 and listed in Table 1. The kinetics of termolecular reactions can be described by the Lindemann-Hinshelwood mechanism whereby the rate constant at the low-pressure limit (k_0 , units in $\text{cm}^6 \text{ molecule}^{-2} \text{ s}^{-1}$) is proportional to the pressure and at the high pressure limit (k_∞ , units in $\text{cm}^3 \text{ molecule}^{-1} \text{ s}^{-1}$) is independent of pressure. In the intermediate pressure range, the fall-off regime, the rate coefficient is a function of both low-pressure (k_0) and high-pressure (k_∞) rate coefficients and the (reaction-partner dependent) broadening factor F which accounts for the lower rate constant measured in the fall-off regime than predicted by the Lindemann-Hinshelwood mechanism reactions (Troe, 1983). Under the conditions of T and p relevant for atmospheric chemistry, the title reaction is in the fall-off regime.

$$k = \frac{k_0[M]k_\infty}{k_0[M] + k_\infty} F \quad (3)$$

125

The solid lines in Figs. 1 and 2 are fits according to the Troe formalism for termolecular reactions (Troe, 1983) as adopted by the IUPAC panel in their evaluation of atmospheric reactions:

$$k(P, T) = \frac{k_0 \left(\frac{T}{300}\right)^{-m} [M] k_\infty \left(\frac{T}{300}\right)^{-n}}{k_0 \left(\frac{T}{300}\right)^{-m} [M] + k_\infty \left(\frac{T}{300}\right)^{-n}} F \quad (4)$$

130 where T is the temperature in Kelvin, $[M]$ is the bath-gas concentration in molecule cm^{-3} , m and n are dimensionless temperature exponents.

The broadening factor, F , is:

$$\log F = \frac{\log F_c}{1 + \left[\log \left(\frac{k_0 \left(\frac{T}{300}\right)^{-m} [M]}{k_\infty \left(\frac{T}{300}\right)^{-n}} \right) / N \right]^2} \quad (5)$$

Where $N = [0.75 - 1.27 \log F_c]$ and F_c is the broadening factor at the centre of the fall-off curve.

135 As discussed in some detail in the first part of our studies of the title reaction (Amedro et al., 2019), the low- or high-pressure rate constants for the title reaction (k_0 and k_∞) are not well defined by existing data sets, which do not deliver sufficiently accurate rate coefficient at very low pressures (< 1 mbar) or at very high pressures (> 500 bar). Studies in which k_∞ has been derived from rates of vibrational relaxation of OH (Smith and Williams, 1985; D'Ottone et al., 2005), return values of k_∞ that provide some constraint on its value, but the associated uncertainty is too large to consider this parameter well defined.

140 In our first paper, Amedro et al. (2019) describe highly accurate measurements of k_1 over a wide range temperatures and pressures in the fall-off regime. From measurements of k_1 in N_2 bath-gas, we retrieved values of k_0 and k_∞ of $2.6 \times 10^{-30} \text{ cm}^6 \text{ molecule}^{-2} \text{ s}^{-1}$ and $6.3 \times 10^{-11} \text{ cm}^3 \text{ molecule}^{-1} \text{ s}^{-1}$, respectively, by fixing F_c to a value of 0.39 which has theoretical basis (Cobos and Troe, 2003). The reasons for choosing this value of F_c are discussed in Amedro et al. (2019). Note that whereas k_0 is dependent on the bath-gas used, at the high-pressure limit, k_∞ should be the same in N_2 , O_2 , He or H_2O bath gases.

145 In Fig.1 we display pressure dependent rate coefficients (solid, black squares) obtained in He bath-gas at 292 K. The black line is a fit (Eqn. 4) to our data with k_∞ fixed to $6.3 \times 10^{-11} \text{ cm}^3 \text{ molecule}^{-1} \text{ s}^{-1}$ and $n = 0$ as derived from an extensive dataset obtained using N_2 bath-gas (Amedro et al., 2019). For this dataset, the best fit is obtained with $F_c = 0.32$, and $k_0^{\text{He}} = 1.4 \times 10^{-30} \text{ cm}^6 \text{ molecule}^{-2} \text{ s}^{-1}$. When using $F_c = 0.39$ (i.e. same value as that obtained in N_2 bath-gas), the fit slightly overestimates ($\sim 5\%$) the measurements at pressures above ~ 300 Torr whereas it underestimates by 10 % at lower pressures (Fig. S2). We note
150 that using a higher $F_c = 0.39$ resulted in a lower value of k_0^{He} equal to $1.0 \times 10^{-30} \text{ cm}^6 \text{ molecule}^{-2} \text{ s}^{-1}$. The T-dependence factor in He, $m(\text{He})$, was determined to be 3.1 over the temperature range from 277 to 332 K (Table 1 and Figure S6).

The high precision of our measurements in He and N₂ indicates that different broadening factors (F_c) are required to interpret the pressure dependence of k_1 obtained in N₂ and He. This can be rationalized by considering that F_c is the product of strong-collision (F_c^{SC}) and weak-collision (F_c^{WC}) components (Eqn. 6-8) (Gilbert et al., 1983; Troe, 1983; Troe and Ushakov, 2011)

$$155 \quad F_c \approx F_c^{SC} F_c^{WC} \quad (6)$$

$$F_c^{SC} \approx S_K^{-0.62} \approx \left(1 + \frac{r}{2}\right)^{-0.62} \quad (7)$$

$$F_c^{WC} \approx \beta_c^{0.14} \quad (8)$$

Here, S_K is the Kassel parameter and r is the total number of external rotational modes of the reactants (equal to 5 in the reaction between OH and NO₂) and β_c is the collision efficiency. While the strong collision component is independent of bath gas (160 ($F_c^{SC} \approx 0.46$ for the title reaction) a change in F_c^{WC} due to a lower collision efficiency (β_c) of He relative to N₂ is likely.

The collision efficiency for N₂ which was used to calculate $F_c = 0.39$ was $\beta_c(\text{N}_2) \approx 0.3$ (Troe, 2001). The value of $F_c = 0.32$ from our He data implies $\beta_c(\text{He}) \approx 0.08$, a factor 3.7 times lower than $\beta_c(\text{N}_2)$. A large difference in collision efficiency between N₂ and He is consistent with theoretical calculations (Glänzer and Troe, 1974; Troe, 2001; Golden et al., 2003).

In Fig 1, we also compare our measurements of k_1 in He with data collected in the same pressure range using similar techniques. (165 The three first measurements (Morley and Smith, 1972; Anastasi and Smith, 1976; Wine et al., 1979) used flash photolysis of H₂O as a OH precursor with detection of OH by resonance fluorescence. Morley and Smith (1972) reported rate coefficients at pressures of 20 to 280 Torr at room temperature with the NO₂ concentration calculated manometrically. Our parametrisation agrees within the combined uncertainty of both measurements (Figure S3). Anastasi and Smith (1976) reported one value of k_1 at 25 Torr He which is $\approx 20\%$ lower than our measurement. Wine et al. (1979) presented values of k_1 at 3 pressures of He. (170 The agreement with our parameterisation at the lowest two pressures is excellent but a deviation of $\approx 20\%$ is observed at the highest pressure (Figure S4). As both studies measured NO₂ concentrations using optical absorption at 365 nm, the $\approx 20\%$ difference is significant. Most recently, D'Ottone et al. (2001) reported rate coefficients from 30 to 600 Torr He using a very similar approach to ours i.e. PLP-LIF technique with in situ measurements of NO₂ by absorption at 365 nm. The disagreement (up to 40%) between our measurements and theirs exceed the combined reported uncertainty (Figure S5). While it is unclear (175 what could have caused the discrepancy, we note that the data of D'Ottone et al. (2001) are significantly more scattered and do not describe a smooth increase in rate coefficient with pressure as expected from termolecular reactions in the fall-off regime. This would appear to indicate an underestimation of the total uncertainty in their study.

Figure 2 extends the pressure range to additionally display data obtained in low pressure flow-tubes (Westenberg and Dehaas, 1972; Anderson et al., 1974; Erlor et al., 1977; Anderson, 1980) and the high-pressure measurements by Hippler et al. (2006). (180 At low pressures our data is in excellent agreement (within 10%) with the data of Erlor et al. (1977) but predict values $\approx 40\%$ lower than those reported by Westenberg and Dehaas (1972) and Anderson (1980). The data of Anderson et al. (1974) display a large intercept ($4.9 \times 10^{-14} \text{ cm}^3 \text{ molecule}^{-1} \text{ s}^{-1}$) at zero pressure, which is attributed to a second-order heterogeneous removal rate constant. As indicated in a critical assessment of the low-pressure data by Amedro et al. (2019) it is unclear whether one can simply subtract a constant value equal to the intercept (obtained from a linear fit) to each data point. If we were to do so, (185 the work by Anderson et al. (1974) would be in very good agreement with the low pressure study by Erlor et al. (1977) as well as with our parametrisation extended to low pressures. Additionally, Amedro et al. (2019) demonstrated that, owing to the large, asymmetric broadening of fall-off for this reaction the assumption that the rate coefficient is in the low pressure limit at N₂ pressures of 0.5 Torr $< p < 10$ Torr is invalid and leads to underestimation of k_0 . This observation is still true of datasets obtained at low pressures of He, so that while very good agreement is observed between our parametrisation and individual (190 rate coefficients obtained between 3 and 8 Torr of He, reported values of k_0^{He} are 40% lower than our values obtained from the fall-off analysis. As indicated in Fig. 2, our parametrisation of k_1 in He is in very good agreement with the high pressure data reported by Hippler et al. (2006).

3.2 Influence of H₂O on k_1

As mentioned above, the effect of water vapour on k_1 was determined in mixtures of H₂O with both N₂ and He. This is because the vapour pressure of H₂O at room temperature (≈ 17 Torr at 293 K) is too low to enable experiments in pure H₂O bath gas to be conducted using our instrument. The measurements were performed at low density ($[M] = 1.6 \times 10^{18}$ molecule cm⁻³; 50 Torr at 293 K) where the relative increase of k_1 in the presence of H₂O is pronounced, resulting in greater accuracy in the determination of $k_0^{\text{H}_2\text{O}}$. Experimental data on the influence of H₂O on k_1 was obtained in N₂-H₂O and He-H₂O mixtures by varying the H₂O mixing ratio, $x_{\text{H}_2\text{O}}$, from 0.05 to 0.27 ($[\text{H}_2\text{O}] = 0.9 - 4.5 \times 10^{17}$ molecule cm⁻³) while keeping the total pressure constant at 50 Torr. Under these conditions, the addition of H₂O resulted in an increase in k_1 up to a factor of two as illustrated by the datasets of Fig. 3 in which the increase in slope as more water-vapour is added is proportional to the increase in k_1 (Eqn. 2). At the highest concentration of water vapour (4.5×10^{17} molecule cm⁻³) the rate coefficient in He-H₂O increased by > factor 3 compared to that obtained in pure He (see Table 1).

In order to determine the temperature dependence of the enhancement in k_1 caused by the presence of water, the experiments in He were carried out at 3 different temperatures (277, 291 and 332 K). The values of k_1 obtained from these experiments are plotted versus the mole-fraction of H₂O in Fig. 4b. At the pressures used in our experiments, k_1 displays fall-off, precluding direct measurement of $k_0^{\text{H}_2\text{O}}$.

The total rate constant measured in e.g. a H₂O-N₂ bath gas is not equal to the sum of the individual rate constants calculated from the mixing ratios of N₂ and H₂O i.e. $k_{\text{N}_2\text{-H}_2\text{O}} \neq k_{\text{N}_2} + k_{\text{H}_2\text{O}}$. $k_{\text{N}_2\text{-H}_2\text{O}}$ is only equal to the sum of k_{N_2} and $k_{\text{H}_2\text{O}}$ at the low pressure limit ($\ll 1$ Torr in the case of the OH reaction with NO₂) and under certain conditions where gas mixtures are composed of strong colliders and/or have similar collision efficiencies (Troe, 1980; Burke and Song, 2017). Additionally, at the high-pressure end of the fall-off curve, the rate coefficient is independent of bath gas composition. To be able to make a reasonable prediction of this effect under atmospheric conditions where the mole fraction of water vapour, $x_{\text{H}_2\text{O}}$, can be as large as 0.05, we analysed our measurements using two different approaches to determine $k_0^{\text{H}_2\text{O}}$. In the first case, the low pressure rate constant in a N₂-H₂O mixture is defined as the sum of two individual low pressure limit rate constants,

$$k(P, T) = \frac{\left(x_{\text{N}_2} k_0^{\text{N}_2} \left(\frac{T}{300}\right)^{-m} + x_{\text{H}_2\text{O}} k_0^{\text{H}_2\text{O}} \left(\frac{T}{300}\right)^{-o}\right) [M] k_\infty \left(\frac{T}{300}\right)^{-n}}{\left(x_{\text{N}_2} k_0^{\text{N}_2} \left(\frac{T}{300}\right)^{-m} + x_{\text{H}_2\text{O}} k_0^{\text{H}_2\text{O}} \left(\frac{T}{300}\right)^{-o}\right) [M] + k_\infty \left(\frac{T}{300}\right)^{-n}} F \quad (9)$$

where x_{N_2} and $x_{\text{H}_2\text{O}}$ are the mixing ratio for N₂ and H₂O respectively, $k_0^{\text{N}_2}$ and $k_0^{\text{H}_2\text{O}}$ are low-pressure limiting rate constants (units of cm⁶ molecule⁻² s⁻¹) for pure N₂ and H₂O, k_∞ is the high-pressure limit rate constant (units of cm³ molecule⁻¹ s⁻¹), T is the temperature in Kelvin, $[M]$ is the molecular density (molecule cm⁻³) and m , n and o are dimensionless temperature exponents.

The broadening factor, F , is:

$$\log F = \frac{\log F_c}{1 + \left[\log \left(\frac{\left(x_{\text{N}_2} k_0^{\text{N}_2} \left(\frac{T}{300}\right)^{-m} + x_{\text{H}_2\text{O}} k_0^{\text{H}_2\text{O}} \left(\frac{T}{300}\right)^{-o}\right) [M]}{k_\infty \left(\frac{T}{300}\right)^{-n}} \right) / N \right]^2} \quad (10)$$

Where $N = [0.75 - 1.27 \log F_c]$ and F_c is the broadening factor at the centre of the fall-off curve.

In the second approach, we follow Burke and Song (2017) where, additionally to the low pressure limiting rate coefficients, the broadening factors for each bath gas are also mixed linearly and $\log F^{\text{N}_2\text{-H}_2\text{O}}$ is defined as

$$\log F^{\text{N}_2\text{-H}_2\text{O}} = \tilde{X}_{\text{N}_2} \log F^{\text{N}_2} + \tilde{X}_{\text{H}_2\text{O}} \log F^{\text{H}_2\text{O}} \quad (11)$$

$$\text{where } \tilde{X}_{\text{N}_2} = \frac{x_{\text{N}_2} k_0^{\text{N}_2} \left(\frac{T}{300}\right)^{-m} [M]}{\left(x_{\text{N}_2} k_0^{\text{N}_2} \left(\frac{T}{300}\right)^{-m} + x_{\text{H}_2\text{O}} k_0^{\text{H}_2\text{O}} \left(\frac{T}{300}\right)^{-o}\right) [M]}; \tilde{X}_{\text{H}_2\text{O}} = \frac{x_{\text{H}_2\text{O}} k_0^{\text{H}_2\text{O}} \left(\frac{T}{300}\right)^{-o} [M]}{\left(x_{\text{N}_2} k_0^{\text{N}_2} \left(\frac{T}{300}\right)^{-m} + x_{\text{H}_2\text{O}} k_0^{\text{H}_2\text{O}} \left(\frac{T}{300}\right)^{-o}\right) [M]} \quad (12)$$

230

$$\log F_c^{N_2} = \frac{\log F_c^{N_2}}{1 + \left[\log \left(\frac{\left(x_{N_2} k_0^{N_2} \left(\frac{T}{300} \right)^{-m} + x_{H_2O} k_0^{H_2O} \left(\frac{T}{300} \right)^{-o} \right) [M]}{k_\infty \left(\frac{T}{300} \right)^{-n}} \right) / (0.75 - 1.27 \log F_c^{N_2}) \right]^2} \quad (13)$$

$$\log F_c^{H_2O} = \frac{\log F_c^{H_2O}}{1 + \left[\log \left(\frac{\left(x_{N_2} k_0^{N_2} \left(\frac{T}{300} \right)^{-m} + x_{H_2O} k_0^{H_2O} \left(\frac{T}{300} \right)^{-o} \right) [M]}{k_\infty \left(\frac{T}{300} \right)^{-n}} \right) / (0.75 - 1.27 \log F_c^{H_2O}) \right]^2} \quad (14)$$

where $F_c^{N_2}$ and $F_c^{H_2O}$ are the broadening factor at the centre of the fall off curve for N_2 and H_2O .

235 In the case where two bath gases have identical (or very similar) values of F_c , the two approaches result in identical predictions and the first approach will be preferred for its simplicity. This is the case for N_2 and H_2O bath gases. However, when two bath-gases have significantly different values of F_c (as is the case for He- H_2O mixtures, see below) the second approach provides a more accurate parameterisation.

3.2.1 Parameterisation of k_1 from data obtained in N_2 - H_2O and He- H_2O bath gases

240 Values of k_1 obtained in N_2 - H_2O and He- H_2O bath gases are listed in Table 2. Each rate coefficient obtained in N_2 - H_2O bath gas was defined by 5 parameters: the mixing ratio of N_2 and H_2O (x_{N_2} and x_{H_2O}) the overall rate coefficient (k_1) the molecular density $[M]$ and the temperature T . We performed a multivariate fit of the N_2 - H_2O dataset with $k_0^{H_2O}$ as variable, all other parameters fixed with: $k_\infty = 6.3 \times 10^{-11} \text{ cm}^3 \text{ molecule}^{-1} \text{ s}^{-1}$, $k_0^{N_2} = 2.6 \times 10^{-30} \text{ cm}^6 \text{ molecule}^{-2} \text{ s}^{-1}$ and $m = 3.6$ as derived in Amedro et al. (2019), o was fixed to 3.4 (see below) and F_c was held at 0.39 making the assumption that the broadening factors at the

245 centre of the fall-off curve for H_2O and N_2 were identical. The fit to the data returned $k_0^{H_2O} = (15.9 \pm 0.7) \times 10^{-30} \text{ cm}^6 \text{ molecule}^{-2} \text{ s}^{-1}$ where the uncertainty is 2σ (statistical only). The solid black line on the upper panel of Fig. 4a represents the parametrisation for a varying fraction of H_2O in N_2 at a total pressure of 50 Torr using the parameters given above. Equating $F_c^{H_2O}$ and $F_c^{N_2}$ simplifies the analysis, though it is likely that $F_c^{H_2O} > F_c^{N_2}$ as the collision efficiency (β_c) is likely to be larger for H_2O than for N_2 . We found that the He- H_2O data cannot be modelled assuming the same F_c for both He and H_2O bath gas

250 and the approach of Burke and Song (2017) was therefore preferred. In order to analyse the data we fixed the following parameters: $k_0^{H_2O} = 15.9 \times 10^{-30} \text{ cm}^6 \text{ molecule}^{-2} \text{ s}^{-1}$, $F_c^{H_2O} = 0.39$, $F_c^{He} = 0.32$ and $k_0^{He} = 1.4 \times 10^{-30} \text{ cm}^6 \text{ molecule}^{-2} \text{ s}^{-1}$ and $m = 3.1$ to derive $o = (3.4 \pm 0.8)$ (2σ , statistical only), which describes the temperature dependence of the low pressure limit in H_2O as depicted in Fig. 4b.

There is clearly some uncertainty related to the arbitrary use of $F_c^{H_2O} = 0.39$. For example, if we were to use analyse the data

255 in N_2 - H_2O using $F_c^{H_2O} = 0.6$ and the linear mixing method we retrieve $k_0^{H_2O} = 10 \times 10^{-30} \text{ cm}^6 \text{ molecule}^{-2} \text{ s}^{-1}$, which is $\approx 50\%$ lower than our preferred value. The effect of the different analyses can be assessed by comparing the predicted impact of H_2O on k_1 at 80% relative humidity, 1000 mbar and 313 K. If we set $F_c^{H_2O} = 0.39$ we predict that the effect of H_2O is to increase k_1 by 15% while choosing $F_c^{H_2O} = 0.6$ results in an increase of 20%. Theoretical calculation of the relative values of F_c in N_2 , O_2 and H_2O bath gases input would be useful to reduce this uncertainty. Our data indicate a significant, positive trend in k_1 when

260 adding H_2O . As discussed above, more efficient energy transfer from $[HO-NO_2]^\#$ in collision with H_2O compared to N_2 is intuitive and supported by the present dataset as well as that of Simonaitis and Heicklen (1972) who derived $k_0^{H_2O} = 11 \times 10^{-30} \text{ cm}^6 \text{ molecule}^{-2} \text{ s}^{-1}$. Given the complexity of the analysis, this may be considered to be in good agreement. This result is however not consistent with the observations of D'Ottone et al. (2001) who report no significant change in k_1 in 150 Torr of He when adding either 10 or 20 Torr of H_2O and is completely at odds with the conclusions of Sadanaga et al. (2006), who report a

265 reduction in k_1 (by 18%) when adding 29.1 mbar of H_2O at atmospheric pressure. If our value for $k_0^{H_2O}$ is correct, D'Ottone et al. (2001) should have seen an increase in k_1 of $\approx 55\%$ and Sadanaga et al. (2006) should have observed an increase of $\approx 5\%$.

A potential explanation for the very divergent observations of the effect of H₂O is the heterogeneous loss of NO₂ when adding H₂O. We tested for NO₂ loss in a set of experiments in which NO₂ and H₂O were monitored simultaneously while systematically varying the amount of H₂O. Our results indicated a reduction in the concentration of NO₂ by up to ≈ 20% as we
270 increased the concentration of H₂O up to 4.5×10^{17} molecule cm⁻³. Unless NO₂ is monitored in-situ (as in our experiments), 20% loss of NO₂ would lead to a similar size reduction in the OH decay constant and thus an underestimation of the rate coefficient. A fractional loss of NO₂ of this magnitude would explain why Sadanaga et al. (2006) found an apparent reduction in k_1 when adding H₂O.

However, the situation becomes more complex if NO₂ is converted to trace gases that are reactive towards OH. For this reason,
275 we performed an additional experiment to investigate whether NO₂ was converted via reaction with H₂O on surfaces to HONO and/or HNO₃. Note that conversion of NO₂ to HONO at low pressures (e.g. 50 Torr) would result in an increase in the OH decay constant ($k_{\text{OH}+\text{HONO}} > k_{\text{OH}+\text{NO}_2}$), whereas conversion of NO₂ to HNO₃ would result in a decrease ($k_{\text{OH}+\text{HNO}_3} < k_{\text{OH}+\text{NO}_2}$).

In order to test for the presence of HONO, we modified the broadband absorption set-up by replacing the halogen lamp with a deuterium lamp, allowing us to detect HONO around 350 nm as well as NO₂. The optical absorption of NO₂ and HONO
280 (340 – 380 nm) was monitored in a flow of NO₂ (1.7×10^{15} cm⁻³) at 50 Torr He in the absence and presence of H₂O ([H₂O] = 4.5×10^{17} molecule cm⁻³, the maximum concentration used in this work). A depletion in NO₂ of 21% (3.7×10^{14} molecule cm⁻³) was observed when H₂O was added. An analysis of the spectra with and without H₂O (Fig. S7) enabled us to establish an upper limit to the HONO concentration of $\approx 1 \times 10^{13}$ molecule cm⁻³, which would correspond to just 3% of the NO₂ lost. At this concentration, HONO does not significantly increase the loss-rate of OH (< 3% using a rate coefficient for reaction of OH
285 with HONO of 6.0×10^{-12} cm³ molecule⁻¹ s⁻¹ (IUPAC, 2019)). In the same experiment, we also recorded the optical density at 185 nm where H₂O, NO₂ and HNO₃ all absorb. Despite the large HNO₃ absorption cross-section at this wavelength (1.6×10^{-17} cm² molecule⁻¹, Dulitz et al. (2018)) we found no evidence for HNO₃ formation, indicating that the NO₂ lost was not converted to gas-phase HNO₃. Given its great affinity for glass in the presence of H₂O, we expect that any HNO₃ formed is strongly partitioned to the walls of the reactor. The tests indicate that, on the time scales of our experiments, NO₂ is lost
290 irreversibly on the humidified walls of our experiment. The maximum concentration of H₂O used in this experiment, 4.5×10^{17} molecule cm⁻³, corresponding to a relative humidity of 80% (at 292 K) so that H₂O condensation is not expected.

It is difficult to establish whether our observations of significant NO₂ loss can explain the result of D'Ottone et al. (2001), who did not observe an enhancement in k_1 . D'Ottone et al. (2001) did not state whether, in their experiments, NO₂ and H₂O were monitored simultaneously. Also, our observed loss of NO₂ is not necessarily transferable to other studies as the heterogeneous
295 loss of NO₂ will vary from one experimental set-up to the next, as residence times and surface areas may vary substantially.

A very simple calculation serves to illustrate the role of water vapour as a third-body quencher for the title reaction. We consider e.g. the tropical boundary layer with a temperature of 30 °C and a relative humidity of 80% at a total pressure of 1 bar. The pressure of water vapour is 34 mbar, those of O₂ and N₂ are then 210 and 756 mbar, respectively. A rough contribution of each quenching gas to the overall rate coefficient can be calculated from the respective low-pressure rate coefficients. For
300 N₂, O₂ and H₂O these are (in units of 10^{-30} cm³ molecule⁻¹ s⁻¹) 2.6, 2.0 and 15.9. Water vapour is therefore a factor ≈ 8 more efficient than O₂, and a factor ≈ 6 more efficient than N₂ as a quencher of the HO-NO₂ intermediate, which is qualitatively consistent with known strong binding (40 kJ mol⁻¹) in the HNO₃-H₂O complex (Tao et al., 1996).

For our tropical boundary layer case-study, in which the O₂ pressure is only a factor of six greater than that of H₂O, we calculate that H₂O contributes more to the rate coefficient of the title reaction than does O₂. Clearly, the neglect of including the
305 quenching effect of H₂O leads to underestimation (in the boundary layer) of the rate coefficient for this centrally important atmospheric reaction.

In order to assess both the effect of H₂O (this work) and the new parameterisation for k_1 in N₂ and O₂ bath-gases presented in first part of this study (Amedro et al., 2019), we have used a 3D chemical transport model (EMAC, see below) to explore the impact on a global scale.

310 3.3. Atmospheric modelling of the OH + NO₂ reaction including the effect of water vapour

The EMAC (ECHAM-MESSy Atmospheric Chemistry) model employed is a numerical chemistry and climate simulation system (Jöckel et al., 2006; Jöckel et al., 2010) using the 5th generation European Centre Hamburg general circulation model (ECHAM5, Roeckner et al. (2006)) as core atmospheric general circulation model. For the present study we applied EMAC (ECHAM5 version 5.3.02, MESSy version 2.53.0) in the T42L47MA-resolution, i.e. with a spherical truncation of T42 (corresponding to a quadratic Gaussian grid of approx. 2.8 by 2.8 degrees in latitude and longitude) with 47 vertical hybrid pressure levels up to 0.01 hPa. The model has been weakly nudged in spectral space, nudging temperature, vorticity, divergence and surface pressure (Jeuken et al., 1996). The chemical mechanism scheme adopted (MOM, Mainz Organic Mechanism) includes oxidation of isoprene, saturated and unsaturated hydrocarbons, including terpenes and aromatics (Sander et al., 2019). Further, tracer emissions and model set-up are similar to the one presented in Lelieveld et al. (2016a). EMAC model predictions have been evaluated against observations on several occasions (Pozzer et al., 2010; de Meij et al., 2012; Elshorbany et al., 2014; Yoon and Pozzer, 2014): For additional references, see <http://www.messy-interface.org>. For this study, EMAC was used in a chemical-transport model (CTM mode) (Deckert et al., 2011), i.e., by disabling feedbacks from photochemistry on radiation and dynamics. Two years were simulated (2009-2010), with the first year used as spin-up time.

The following parameterisation of k_1 was implemented in EMAC; values of each parameter are listed in Table 3.

325

$$k_1(P, T) = \frac{\left(x_{\text{N}_2}k_0^{\text{N}_2}\left(\frac{T}{300}\right)^{-m} + x_{\text{O}_2}k_0^{\text{O}_2}\left(\frac{T}{300}\right)^{-q} + x_{\text{H}_2\text{O}}k_0^{\text{H}_2\text{O}}\left(\frac{T}{300}\right)^{-o}\right)Mk_\infty\left(\frac{T}{300}\right)^{-n}}{\left(x_{\text{N}_2}k_0^{\text{N}_2}\left(\frac{T}{300}\right)^{-m} + x_{\text{O}_2}k_0^{\text{O}_2}\left(\frac{T}{300}\right)^{-q} + x_{\text{H}_2\text{O}}k_0^{\text{H}_2\text{O}}\left(\frac{T}{300}\right)^{-o}\right)M+k_\infty\left(\frac{T}{300}\right)^{-n}}F \quad (15)$$

The broadening factor, $\log F$, is:

$$\log F = \frac{\log F_c}{1 + \left[\log \left(\frac{\left(x_{\text{N}_2}k_0^{\text{N}_2}\left(\frac{T}{300}\right)^{-m} + x_{\text{O}_2}k_0^{\text{O}_2}\left(\frac{T}{300}\right)^{-q} + x_{\text{H}_2\text{O}}k_0^{\text{H}_2\text{O}}\left(\frac{T}{300}\right)^{-o}\right)M}{k_\infty\left(\frac{T}{300}\right)^{-n}} \right) / [0.75 - 1.27 \log F_c] \right]^2} \quad (16)$$

330 As described in Section 1, the reaction between OH and NO₂ forms not only HNO₃ but also HOONO. HOONO decomposes rapidly at typical boundary layer temperatures but is long lived with respect to thermal dissociation at the temperatures found in the upper troposphere and lower stratosphere (UTLS).



The rate constant (k_6) for thermal decomposition of HOONO was calculated from the channel specific rate coefficient for its formation ($k_1\alpha$) and an equilibrium coefficient: $k_6 = k_1\alpha / K_{\text{eq}}$, where $K_{\text{eq}} = 3.5 \times 10^{-27} \exp(10135/T)$ (Burkholder et al., 2015; IUPAC, 2019) based on the analysis of (Golden et al., 2003). The branching ratio to HOONO formation (α) was adapted from the present IUPAC recommendations for k_{1a} and k_{1b} which were derived from experimental work (Hippler et al., 2006; Mollner et al., 2010) and theoretical analysis (Troe, 2012). The IUPAC recommendations were augmented with a pressure independent HOONO yield of 0.035 to better represent the dataset of Mollner et al. (2010) who detected HOONO directly at room temperature. We assume α is independent of water vapour. The expression used and a plot of α at different temperatures and pressures is given in Fig. S8 of the supplementary information.

In the absence of experimental data on the reactions of HOONO with OH or on its photolysis, we follow the approach of Golden and Smith (2000) and set these equal to those for HO₂NO₂ :



In Fig. 5, we illustrate the global impact (annual average) of H₂O-vapour on the rate coefficient. We plot the fractional reduction in k_1 at the Earth's surface when setting $x_{\text{H}_2\text{O}}$ to zero rather than using the EMAC global water-vapour fields. We focus on the boundary layer as the H₂O concentration is largest here and decreases rapidly with altitude.

As expected, the greatest effect is found in warm, tropical regions where neglecting the impact of water vapour results in an average underestimation of the rate coefficient by up to $\approx 8\%$. At higher/lower latitudes the effect is diminished and water vapour accounts for only 3-4 % of the overall rate coefficient at 40° N/S. The presence of water vapour does not impact on values of k_1 above the boundary layer.

Our experimental data do not give insight into whether the H₂O-induced enhancement in k_1 is accompanied by a change in the branching ratio to favour either HNO₃ or HOONO. However, as the formation of HOONO is favoured at high pressures (more effective collisional deactivation) it is possible that the HOONO yield may be enhanced relative to HNO₃ in the presence of H₂O. If this is the case, the increase in rate coefficient at high water vapour levels (e.g. in the tropical lower troposphere) may be to some extent offset by the subsequent thermal dissociation of HOONO in these warm regions.

As described by Amedro et al. (2019) (Fig. 1 of their manuscript) two expert panels (IUPAC, NASA) evaluating kinetic data for use in atmospheric modelling fail to reach consensus for the title reaction, with the preferred rate coefficients differing by as much as 50% in the cold UTLS. For this reason we have calculated values of $\frac{k_1^{\text{NASA}}}{k_1^{\text{this work}}}$ and $\frac{k_1^{\text{IUPAC}}}{k_1^{\text{this work}}}$ at different altitudes and latitudes (i.e. at different temperatures and pressures). We parameterized the rate coefficient using the expressions given in this work (Eqn. 15, Table 3) and in the latest evaluations of IUPAC (k_1 last evaluated in 2017 (IUPAC, 2019)) and NASA (last evaluation published in 2015 (Burkholder et al., 2015)). As displayed in Fig. 6, values of $\frac{k_1^{\text{NASA}}}{k_1^{\text{this work}}}$ and $\frac{k_1^{\text{IUPAC}}}{k_1^{\text{this work}}}$ vary greatly with pressure and temperature and thus altitude. The NASA recommendations are always slightly lower but in good agreement ($\leq 10\%$) for most of the troposphere, with larger differences ($(\frac{k_1^{\text{NASA}}}{k_1^{\text{this work}}})$ always < 1) only observed in the lower and mid-stratosphere. At altitudes above ≈ 30 km the ratio decreases to ≈ 0.8 . A comparison with the rate coefficient derived from the IUPAC parameterization, shows that $\frac{k_1^{\text{IUPAC}}}{k_1^{\text{this work}}}$ varies from ≈ 0.9 at the surface to ≈ 1.1 at the tropopause but increases to >1.3 at the low pressures and temperatures that reign at 30 km and above. At high altitudes (low pressure and temperature) the rate coefficients that the evaluation panels recommend are strongly biased by choice of the rate coefficient (and its temperature dependence) at the low pressure limit. As discussed by Amedro et al. (2019) the available experimental data at low pressures and temperature are not of sufficient accuracy to use as basis for recommendation of k_0 and this is reflected in the highly divergent values of k_1 under these conditions.

As mentioned above, the atmospheric HNO₃ / NO₂ ratio is expected to be highly sensitive to the rate coefficient k_1 , with an increase in k_1 resulting in an increase in the HNO₃ / NO₂ ratio and vice versa. The HNO₃ / NO₂ ratio also depends on the concentration of OH and thus the effect of using different values of k_1 will be most apparent in regions where the greatest OH concentrations are found, i.e. at low latitudes. At higher latitudes, especially in winter months where solar insolation is weak and OH levels are relatively low, the HNO₃ / NO₂ ratio will also be impacted by nighttime conversion of NO₂ to N₂O₅ and finally, via heterogeneous hydrolysis, to HNO₃. In Fig. 7 we plot zonally and yearly averaged model values of $\frac{\text{HNO}_3}{\text{NO}_2}$ (IUPAC) / $\frac{\text{HNO}_3}{\text{NO}_2}$ (this work) in the upper panel and $\frac{\text{HNO}_3}{\text{NO}_2}$ (NASA) / $\frac{\text{HNO}_3}{\text{NO}_2}$ (this work) in the lower panel. Compared to the present parameterization of k_1 , the IUPAC evaluation returns HNO₃ / NO₂ ratios that are between 0.9 and 1 throughout most of the lower and free-troposphere (up to ≈ 5 km) and larger HNO₃ / NO₂ ratios (factor of 1.1 to 1.15) above ≈ 10 km especially at the tropical tropopause. The divergence between the HNO₃ / NO₂ ratios increases as we move further into the stratosphere with $\frac{\text{HNO}_3}{\text{NO}_2}$ (IUPAC) / $\frac{\text{HNO}_3}{\text{NO}_2}$ (this work) as large as 1.2 to 1.3 above 25 km. At the same time, NO_x levels (NO_x = NO + NO₂) decrease by a factor ≈ 0.95 (see Fig. S9 of the supplementary information). When we compare our parameterization with that of the NASA panel, the picture is largely reversed (lower panel). Again, we find reasonable agreement in the HNO₃ / NO₂ ratio in the lowermost atmosphere, but in this case lower values (0.8 to 0.9) in the lower stratosphere which are accompanied by a factor 1.06 change in NO_x concentrations (Fig. S9). For both the NASA and IUPAC parameterizations, the largest differences in the HNO₃ / NO₂ ratio compared to the present study are found higher in the atmosphere. The modelling studies confirm the

390 simple calculation of Amedro et al. (2019) (see Fig. 1 of their paper), showing that the IUPAC and NASA parameterizations
result in very different values of k_1 in some parts of the atmosphere and will result in divergent predictions of partitioning of
reactive nitrogen between NO_x and NO_y . Use of the parameterization based on the present dataset lies roughly between the
two evaluations, with best agreement observed with NASA for the lower atmosphere. However, as previous laboratory studies
had not identified the important role of H_2O in the title reaction, which could therefore not be incorporated in either of the
previous parameterizations, any agreement at better than 10% level is fortuitous, reflecting random cancelling of systematic
395 bias.

As reaction with OH is the predominant sink for most atmospheric trace-gases, its concentration largely defines the oxidizing
power of the atmosphere (Lelieveld et al., 2004; Lelieveld et al., 2008; Lelieveld et al., 2016b) and even changes of a few
percent in its concentration are significant. An increase in the rate coefficient of the title reaction will reduce the atmospheric
abundance of this centrally important radical. In Fig. S10 we illustrate the impact of using the parameterization of k_1 from the
400 present study compared to the IUPAC and NASA recommendations. The upper panel in Fig. S10 plots the ratio of OH
concentrations obtained when using the IUPAC parameterization and that from the present study, $\text{OH(IUPAC)} / \text{OH(this work)}$.
Throughout the troposphere $\text{OH(IUPAC)} / \text{OH(this work)}$ deviates by only a few percent, with a value of 1.02 at the
surface and 0.96 at the tropical tropopause. $\text{OH(NASA)} / \text{OH(this work)}$ is also 1.02 at the surface but increases to 1.04 at the
tropical tropopause as the NASA-derived value of k_1 is lower at the temperatures and pressures encountered in this part of the
405 atmosphere. The weak effect of changing k_1 on OH at the surface reflects the fact that many reactions apart from that with NO_2
contribute to the overall sink term for OH in the lower troposphere.

Although our experiments do not give insight into the branching between formation of HOONO and HNO_3 in the title reaction,
previous work predicts a significant yield of HOONO especially at low temperatures (see Fig S8). As the lifetime of HOONO
with respect to re-dissociation to reactants is short at e.g. boundary layer temperatures (≈ 1 s at 298 K and 1 bar pressure), its
410 formation may be seen as an effective reduction in the rate coefficient for $\text{OH} + \text{NO}_2$ (Golden and Smith, 2000). However, its
lifetime increases to several days at temperature and pressure conditions typical e.g. of the tropical tropopause (100 mbar, 220
K). As HOONO formation and loss are now parameterized (see above) in EMAC, we can explore its potential contribution to
odd-nitrogen species in the atmosphere. The reaction between OH and NO_2 to form HOONO converts short lived HO $_x$ (HO $_x$
= $\text{OH} + \text{HO}_2$) and NO_x ($\text{NO}_x = \text{NO} + \text{NO}_2$) into a longer lived “reservoir” species, and in this sense is similar to the reaction
415 between HO_2 and NO_2 to form HO_2NO_2



which is also thermally unstable, dissociating to reform HO_2 and NO_2 . Unlike HOONO, for which there are no atmospheric
measurements, much effort has been made to measure concentrations of HO_2NO_2 in colder regions of the atmosphere and it is
considered an important component of the NO_y budget at high altitudes (Nault et al., 2016). We therefore compared EMAC
420 predictions of HOONO concentrations with those of HO_2NO_2 . The results are displayed in Fig. 8, in which we plot the zonally
averaged HOONO / HO_2NO_2 ratio. Immediately apparent from Fig. 8 is that, compared to HO_2NO_2 , HOONO is a minor
component of NO_y in the warm, lower atmosphere. This reflects the difference in the thermal decomposition rate constant of
the two trace gases, that of HO_2NO_2 being $\approx 4 \times 10^{-5} \text{ s}^{-1}$ in e.g. the middle troposphere at 400 mbar and 250 K, whereas
HOONO decomposes a factor 30 faster so that its lifetime is only ≈ 1000 s. In the UTLS region, the ratio increases further
425 (HO_2NO_2 is a factor 50 more long-lived w.r.t. thermal decomposition at 100 mbar and 220 K) but the lifetimes of both gases
under these conditions are sufficiently long that their concentrations are largely determined by their production rates and their
losses due to photolysis and reaction with OH. The maximum ratio of HOONO to HO_2NO_2 is found at the tropical tropopause,
where concentrations become comparable. As the modelled loss processes of HOONO and HO_2NO_2 (rate constants for
photolysis and reaction with OH) are assumed to be identical, the occurrence of the maximum HOONO to HO_2NO_2 ratio at
430 the tropical tropopause is related to the ratio of the (temperature dependent) rate coefficients responsible for their formation
(at 220 K and 100 mbar this favours HOONO formation by a factor of ≈ 2) and the model OH / HO_2 ratio. Whilst this result

indicates that HOONO could be an important reservoir of NO_x under certain conditions, we must bear in mind that there is great uncertainty associated not only with the branching ratio to HOONO formation in R1b but also with its loss processes (reaction with OH, photolysis), which remain unexplored experimentally. OH reacts with HO₂NO₂ via H-abstraction from the H-OO group (IUPAC, 2019), and a similar mechanism is likely for HOONO. As the H-OO bond strength is likely to be greater in HOONO than in HO₂NO₂ (larger electron density around the peroxy bond) we may expect the rate coefficient to be lower for HOONO. A significantly lower rate coefficient for reaction with OH (or photolysis rate constant) could greatly increase the abundance of HOONO. If this were the case, airborne instruments that measure NO_x would likely also measure some fraction of HOONO following its rapid decomposition in warm inlet lines, as has been observed for HO₂NO₂ and CH₃O₂NO₂ (Nault et al., 2015; Silvern et al., 2018). Clearly, more experimental or theoretical data that better constrain the yield of HOONO and its atmospheric loss processes as well as atmospheric measurements are necessary in order to improve our understanding of the role of the reaction between OH and NO₂ throughout the atmosphere.

4 Conclusions

We have made very precise and accurate measurements for the overall rate coefficient, k_1 , of the reaction between OH and NO₂, which is of critical importance in atmospheric chemistry. Our experiments demonstrate clearly that the presence of H₂O increases significantly the overall rate coefficient (k_1) of the reaction between OH and NO₂. H₂O is found to be a more efficient collisional quencher (by a factor of ≈ 6) of the initially formed HO-NO₂ association complex than N₂ and a factor ≈ 8 more efficient than O₂. A new parameterisation of the rate coefficient for the title reaction that considers the roles of N₂, O₂ and H₂O as third-body quenchers (also using data from our companion paper, Amedro et al. (2019)) has been incorporated into a global, chemistry transport model to assess its impact on e.g. the HNO₃ / NO₂ ratio as well as NO_x and OH levels. Compared to existing evaluations of the kinetic data, use of the new parameters will result in significant changes (5-10%) in the partitioning of NO_x and NO_y, the direction of the bias depending on which evaluation is used as reference and on region of the atmosphere. This work highlights the continuing importance of obtaining accurate laboratory kinetic data for those reactions that are central to our understanding of atmospheric chemistry and which provide anchor-points in chemical transport models. Though the result is associated with great uncertainty owing to missing kinetic parameters for HOONO, the global model predicts the presence of HOONO in concentrations similar to those of HO₂NO₂ at the tropical tropopause. The present dataset addresses only the overall rate coefficient, k_1 . Detailed experimental studies of the formation of HOONO (e.g. its yield at various temperatures and in the presence of H₂O) and on the fate of HOONO (OH kinetics, photolysis) are required to better assess its role as NO_x and HO_x reservoir in cold parts of the atmosphere.

460

Data availability. The rate coefficients measured during this experimental study are listed in Table 1.

Author contributions. The experiments were carried out by DA, AJCB, and MB. The data analysis and preparation of the paper were performed by DA, with assistance from JL and JNC. The global modelling was performed by AP.

Competing interests. The authors declare that they have no conflict of interest.

465 *Financial support.* The article processing charges for this open access publication were covered by the Max Planck Society.

References

- 470 Allodi, M. A., Dunn, M. E., Livada, J., Kirschner, K. N., and Shields, G. C.: Do hydroxyl radical-water clusters, $\text{OH}(\text{H}_2\text{O})(n)$, $n=1-5$, exist in the atmosphere?, *J. Phys. Chem. A*, 110, 13283-13289, doi:10.1021/jp064468l, 2006.
- Amedro, D., Bunkan, A. J. C., Berasategui, M., and Crowley, J. N.: Kinetics of the $\text{OH} + \text{NO}_2$ reaction: rate coefficients (217–333 K, 16–1200mbar) and fall-off parameters for N_2 and O_2 bath gases, *Atmos. Chem. Phys.*, 19, 10643-10657, doi:10.5194/acp-19-10643-2019, 2019.
- Anastasi, C., and Smith, I. W. M.: Rate measurements of reactions of OH by resonance absorption. Part 5.-Rate constants for $\text{OH} + \text{NO}_2 (+\text{M}) \rightarrow \text{HNO}_3 (+\text{M})$ over a wide range of temperature and pressure, *Journal of the Chemical Society, Faraday Transactions 2: Molecular and Chemical Physics*, 72, 1459-1468, doi:10.1039/f29767201459, 1976.
- 475 Anderson, J. G., Margitan, J. J., and Kaufman, F.: Gas-phase recombination of OH with NO and NO_2 , *J. Chem. Phys.*, 60, 3310-3317, 1974.
- Anderson, L. G.: Absolute rate constants for the reaction of OH with NO_2 in N_2 and He from 225 to 389 K, *J. Phys. Chem.*, 84, 2152-2155, 1980.
- Burke, M. P., and Song, R.: Evaluating mixture rules for multi-component pressure dependence: $\text{H} + \text{O}_2 (+\text{M}) = \text{HO}_2 (+\text{M})$, *Proceedings of the Combustion Institute*, 36, 245-253, doi:<https://doi.org/10.1016/j.proci.2016.06.068>, 2017.
- 480 Burkholder, J. B., Sander, S. P., Abbatt, J., Barker, J. R., Huie, R. E., Kolb, C. E., Kurylo, M. J., Orkin, V. L., Wilmouth, D. M., and Wine, P. H.: Chemical Kinetics and Photochemical Data for Use in Atmospheric Studies, Evaluation No. 18," JPL Publication 15-10, Jet Propulsion Laboratory, Pasadena, <http://jpldataeval.jpl.nasa.gov>, 2015.
- Buszek, R. J., Francisco, J. S., and Anglada, J. M.: Water effects on atmospheric reactions, *International Reviews in Physical Chemistry*, 30, 335-369, doi:10.1080/0144235X.2011.634128, 2011.
- 485 Cantrell, C. A., Zimmer, A., and Tyndall, G. S.: Absorption cross sections for water vapor from 183 to 193 nm, *Geophys. Res. Lett.*, 24, 2195-2198, 1997.
- Cobos, C. J., and Troe, J.: Prediction of reduced falloff curves for recombination reactions at low temperatures, *Z. Phys. Chem.*, 217, 1031-1044, 2003.
- 490 D'Ottone, L., Campuzano-Jost, P., Bauer, D., and Hynes, A. J.: A pulsed laser photolysis-pulsed laser induced fluorescence study of the kinetics of the gas-phase reaction of OH with NO_2 , *J. Phys. Chem. A*, 105, 10538-10543, 2001.
- D'Ottone, L., Bauer, D., Campuzano-Jost, P., Fardy, M., and Hynes, A. J.: Kinetic and mechanistic studies of the recombination of OH with NO_2 : Vibrational deactivation, isotopic scrambling and product isomer branching ratios, *Faraday Discussions*, 130, 111-123, 2005.
- de Meij, A., Pozzer, A., Pringle, K. J., Tost, H., and Lelieveld, J.: EMAC model evaluation and analysis of atmospheric aerosol properties and distribution with a focus on the Mediterranean region, *Atmospheric Research*, 114, 38-69, 2012.
- 495 Deckert, R., Jockel, P., Grewe, V., Gottschaldt, K. D., and Hoor, P.: A quasi chemistry-transport model mode for EMAC, *Geoscientific Model Development*, 4, 195-206, 2011.
- Dulitz, K., Amedro, D., Dillon, T. J., Pozzer, A., and Crowley, J. N.: Temperature-(208-318 K) and pressure-(18-696 Torr) dependent rate coefficients for the reaction between OH and HNO_3 , *Atmos. Chem. Phys.*, 18, 2381-2394, 2018.
- 500 Elshorbany, Y. F., Crutzen, P. J., Steil, B., Pozzer, A., Tost, H., and Lelieveld, J.: Global and regional impacts of HONO on the chemical composition of clouds and aerosols, *Atmos. Chem. Phys.*, 14, 1167-1184, 2014.
- Erler, K., Field, D., Zellner, R., and Smith, I. W. M.: Recombination reaction between hydroxyl radicals and nitrogen-dioxide: $\text{OH} + \text{NO}_2 + \text{M} (= \text{He}, \text{CO}_2)$ in temperature range 213-300K, *Berichte Der Bunsen-Gesellschaft-Physical Chemistry Chemical Physics*, 81, 22-26, doi:10.1002/bbpc.19770810107, 1977.
- 505 Fernandes, R. X., Luther, K., Troe, J., and Ushakov, V. G.: Experimental and modelling study of the recombination reaction $\text{H} + \text{O}_2 (+\text{M}) \rightarrow \text{HO}_2 (+\text{M})$ between 300 and 900 K, 1.5 and 950 bar, and in the bath gases $\text{M} = \text{He}, \text{Ar},$ and N_2 , *Phys. Chem. Chem. Phys.*, 10, 4313-4321, doi:10.1039/b804553d, 2008.
- Getzinger, R. W., and Blair, L. S.: Recombination in the hydrogen-oxygen reaction: A shock tube study with nitrogen and water vapour as third bodies, *Combust. Flame*, 13, 271-284, doi:[https://doi.org/10.1016/0010-2180\(69\)90005-4](https://doi.org/10.1016/0010-2180(69)90005-4), 1969.
- 510 Gilbert, R. G., Luther, K., and Troe, J.: Theory of thermal unimolecular reactions in the fall-off range .2. weak collision rate constants, *Berichte Der Bunsen-Gesellschaft-Physical Chemistry Chemical Physics*, 87, 169-177, 1983.
- Glänzer, K., and Troe, J.: Thermal Decomposition of Nitrocompounds in Shock Waves. IV: Decomposition of Nitric Acid, *Berichte der Bunsengesellschaft für physikalische Chemie*, 78, 71-76, doi:10.1002/bbpc.19740780112, 1974.
- Golden, D. M., and Smith, G. P.: Reaction of $\text{OH} + \text{NO}_2 + \text{M}$: A new view, *J. Phys. Chem. A*, 104, 3991-3997, 2000.
- 515 Golden, D. M., Barker, J. R., and Lohr, L. L.: Master equation models for the pressure- and temperature-dependant reactions $\text{HO} + \text{NO}_2 \rightarrow \text{HONO}_2$ and $\text{HO} + \text{NO}_2 \rightarrow \text{HOONO}$, *J. Phys. Chem. A*, 107, 11057-11071, 2003.
- Hippler, H., Krasteva, N., Nasterlack, S., and Striebel, F.: Reaction of OH + NO_2 : High pressure experiments and falloff analysis, *J. Phys. Chem. A*, 110, 6781-6788, 2006.
- IUPAC: Task Group on Atmospheric Chemical Kinetic Data Evaluation, (Ammann, M., Cox, R.A., Crowley, J.N., Herrmann, H., Jenkin, M.E., McNeill, V.F., Mellouki, A., Rossi, M. J., Troe, J. and Wallington, T. J.) <http://iupac.pole-ether.fr/index.html>, 2019.
- 520 Jeuken, A. B. M., Siegmund, P. C., Heijboer, L. C., Feichter, J., and Bengtsson, L.: On the potential of assimilating meteorological analyses in a global climate model for the purpose of model validation, *J. Geophys. Res. -Atmos.*, 101, 16939-16950, 1996.
- Jöckel, P., Tost, H., Pozzer, A., Bruhl, C., Buchholz, J., Ganzeveld, L., Hoor, P., Kerkweg, A., Lawrence, M. G., Sander, R., Steil, B., Stiller, G., Tanarhte, M., Taraborrelli, D., Van Aardenne, J., and Lelieveld, J.: The atmospheric chemistry general circulation model ECHAM5/MESSy1: consistent simulation of ozone from the surface to the mesosphere, *Atmos. Chem. Phys.*, 6, 5067-5104, 2006.
- 525 Jöckel, P., Kerkweg, A., Pozzer, A., Sander, R., Tost, H., Riede, H., Baumgaertner, A., Gromov, S., and Kern, B.: Development cycle 2 of the Modular Earth Submodel System (MESSy2), *Geoscientific Model Development*, 3, 717-752, 2010.
- Kircher, C. C., and Sander, S. P.: Kinetics and mechanism of HO_2 and DO_2 disproportionations, *J. Phys. Chem.*, 88, 2082-2091, 1984.
- Lelieveld, J., Dentener, F. J., Peters, W., and Krol, M. C.: On the role of hydroxyl radicals in the self-cleansing capacity of the troposphere, *Atmos. Chem. Phys.*, 4, 2337-2344, 2004.
- 530 Lelieveld, J., Butler, T. M., Crowley, J. N., Dillon, T. J., Fischer, H., Ganzeveld, L., Harder, H., Lawrence, M. G., Martinez, M., Taraborrelli, D., and Williams, J.: Atmospheric oxidation capacity sustained by a tropical forest, *Nature*, 452, 737-740, 2008.
- Lelieveld, J., Gromov, S., Pozzer, A., and Taraborrelli, D.: Global tropospheric hydroxyl distribution, budget and reactivity, *Atmos. Chem. Phys.*, 16, 12477-12493, 2016a.
- 535 Lelieveld, J., Gromov, S., Pozzer, A., and Taraborrelli, D.: Global tropospheric hydroxyl distribution, budget and reactivity, *Atmos. Chem. Phys. Discuss.*, 2016, 1-25, doi:10.5194/acp-2016-160, 2016b.

- Lii, R.-R., Sauer, M. C., and Gordon, S.: Temperature dependence of the gas-phase self-reaction of HO₂ in the presence of H₂O, *J. Phys. Chem.*, 85, 2833-2834, 1981.
- 540 Michael, J. V., Su, M. C., Sutherland, J. W., Carroll, J. J., and Wagner, A. F.: Rate constants for H+O₂+M → HO₂+M in seven bath gases, *J. Phys. Chem. A*, 106, 5297-5313, doi:10.1021/jp020229w, 2002.
- Mollner, A. K., Valluvadasan, S., Feng, L., Sprague, M. K., Okumura, M., Milligan, D. B., Bloss, W. J., Sander, S. P., Martien, P. T., Harley, R. A., McCoy, A. B., and Carter, W. P. L.: Rate of gas phase association of hydroxyl radical and nitrogen dioxide, *Science*, 330, 646-649, doi:10.1126/science.1193030, 2010.
- 545 Morley, C., and Smith, I. W. M.: Rate measurements of reactions of OH by resonance absorption. 1. Reactions of OH with NO₂ and NO, *Journal of the Chemical Society-Faraday Transactions II*, 68, 1016-&, doi:10.1039/f29726801016, 1972.
- Nault, B. A., Garland, C., Pusede, S. E., Wooldridge, P. J., Ullmann, K., Hall, S. R., and Cohen, R. C.: Measurements of CH₃O₂NO₂ in the upper troposphere, *Atmos. Meas. Tech.*, 8, 987-997, doi:doi:10.5194/amt-8-987-2015, 2015.
- Nault, B. A., Garland, C., Wooldridge, P. J., Brune, W. H., Campuzano-Jost, P., Crouse, J. D., Day, D. A., Dibb, J., Hall, S. R., Huey, L. G., Jimenez, J. L., Liu, X. X., Mao, J. Q., Mikoviny, T., Peischl, J., Pollack, I. B., Ren, X. R., Ryerson, T. B., Scheuer, E., Ullmann, K., 550 Wennberg, P. O., Wisthaler, A., Zhang, L., and Cohen, R. C.: Observational Constraints on the Oxidation of NO_x in the Upper Troposphere, *J. Phys. Chem. A*, 120, 1468-1478, doi:10.1021/acs.jpca.5b07824, 2016.
- Newsome, B., and Evans, M.: Impact of uncertainties in inorganic chemical rate constants on tropospheric composition and ozone radiative forcing, *Atmos. Chem. Phys.*, 17, 14333-14352, doi:10.5194/acp-17-14333-2017, 2017.
- 555 Pozzer, A., Pollmann, J., Taraborrelli, D., Jockel, P., Helmig, D., Tans, P., Hueber, J., and Lelieveld, J.: Observed and simulated global distribution and budget of atmospheric C-2-C-5 alkanes, *Atmos. Chem. Phys.*, 10, 4403-4422, 2010.
- Roeckner, E., Brokopf, R., Esch, M., Giorgetta, M., Hagemann, S., Kornblueh, L., Manzini, E., Schlese, U., and Schulzweida, U.: Sensitivity of simulated climate to horizontal and vertical resolution in the ECHAM5 atmosphere model, *Journal of Climate*, 19, 3771-3791, 2006.
- Sadanaga, Y., Kondo, S., Hashimoto, K., and Kajii, Y.: Measurement of the rate coefficient for the OH+NO₂ reaction under the atmospheric pressure: Its humidity dependence, *Chem. Phys. Lett.*, 419, 474-478, 2006.
- 560 Sander, R., Baumgaertner, A., Cabrera-Perez, D., Frank, F., Gromov, S., Grooss, J. U., Harder, H., Huijnen, V., Jockel, P., Karydis, V. A., Niemeyer, K. E., Pozzer, A., Hella, R. B., Schultz, M. G., Taraborrelli, D., and Tauer, S.: The community atmospheric chemistry box model CAABA/MECCA-4.0, *Geoscientific Model Development*, 12, 1365-1385, doi:10.5194/gmd-12-1365-2019, 2019.
- Shao, J., Choudhary, R., Susa, A., Davidson, D. F., and Hanson, R. K.: Shock tube study of the rate constants for H + O₂ + M → HO₂ + M (M = Ar, H₂O, CO₂, N₂) at elevated pressures, *Proceedings of the Combustion Institute*, 37, 145-152, 565 doi:<https://doi.org/10.1016/j.proci.2018.05.077>, 2019.
- Silvern, R. F., Jacob, D. J., Travis, K. R., Sherwen, T., Evans, M. J., Cohen, R. C., Laughner, J. L., Hall, S. R., Ullmann, K., Crouse, J. D., Wennberg, P. O., Peischl, J., and Pollack, I. B.: Observed NO/NO₂ ratios in the upper troposphere imply errors in NO-NO₂-O₃ cycling kinetics or an unaccounted NO_x reservoir, *Geophys. Res. Lett.*, 45, 4466-4474, doi:10.1029/2018gl077728, 2018.
- 570 Simonaitis, R., and Heicklen, J.: The reaction of OH with NO₂ and the deactivation of O(¹D) by CO, *Int. J. Chem. Kinet.*, IV, 529-540, 1972.
- Smith, I. W., and Williams, M. D.: Vibrational-relaxation of OH(v=1) and OD(v=1) By HNO₃, DNO₃, H₂O, NO and NO₂, *Journal of the Chemical Society, Faraday Transactions 2: Molecular and Chemical Physics*, 81, 1849-1860, 1985.
- Tao, F. M., Higgins, K., Klemperer, W., and Nelson, D. D.: Structure, binding energy, and equilibrium constant of the nitric acid-water complex, *Geophys. Res. Lett.*, 23, 1797-1800, 1996.
- 575 Thomsen, D. L., Kurten, T., Jorgensen, S., Wallington, T. J., Baggesen, S. B., Aalling, C., and Kjaergaard, H. G.: On the possible catalysis by single water molecules of gas-phase hydrogen abstraction reactions by OH radicals, *Phys. Chem. Chem. Phys.*, 14, 12992-12999, doi:10.1039/c2cp40795g, 2012.
- Troe, J.: Mixture Rules in Thermal Unimolecular Reactions, *Berichte der Bunsengesellschaft für physikalische Chemie*, 84, 829-834, doi:10.1002/bbpc.19800840902, 1980.
- 580 Troe, J.: Theory of thermal unimolecular reactions in the fall-off range 1. Strong collision rate constants, *Berichte Der Bunsen-Gesellschaft-Physical Chemistry Chemical Physics*, 87, 161-169, 1983.
- Troe, J.: Analysis of the temperature and pressure dependence of the reaction HO+NO₂+M → HONO₂+M, *Int. J. Chem. Kinet.*, 33, 878-889, 2001.
- Troe, J.: Toward a Quantitative Analysis of Association Reactions in the Atmosphere, *Chem. Rev.*, 103, 4565-4576, doi:10.1021/cr020514b, 2003.
- 585 Troe, J., and Ushakov, V. G.: Revisiting falloff curves of thermal unimolecular reactions, *The Journal of Chemical Physics*, 135, 054304, doi:10.1063/1.3615542, 2011.
- Troe, J.: Refined representation of falloff curves for the reaction HO + NO₂ + N₂ → (HONO₂, HOONO) + N₂, *J. Phys. Chem. A*, 116, 6387-6393, doi:10.1021/jp212095n, 2012.
- 590 Vandaele, A. C., Hermans, C., Fally, S., Carleer, M., Colin, R., Merienne, M. F., Jenouvrier, A., and Coquart, B.: High-resolution Fourier transform measurement of the NO₂ visible and near-infrared absorption cross sections: Temperature and pressure effects, *J. Geophys. Res. -Atmos.*, 107, Art. 4348, doi:10.1029/2001JD000971, 2002.
- Westenberg, A. A., and Dehaas, N.: Rate measurements on OH+NO+M and OH+NO₂+M, *J. Chem. Phys.*, 57, 5375-+, doi:10.1063/1.1678234, 1972.
- 595 Wine, P. H., Kreutter, N. M., and Ravishankara, A. R.: Flash photolysis-resonance fluorescence kinetics study of the reaction OH + NO₂ + M → HNO₃ + M, *J. Phys. Chem.*, 83, 3191-3195, 1979.
- Wollenhaupt, M., Carl, S. A., Horowitz, A., and Crowley, J. N.: Rate coefficients for reaction of OH with acetone between 202 and 395 K, *J. Phys. Chem.*, 104, 2695-2705, doi:10.1021/jp993738f, 2000.
- 600 Yoon, J., and Pozzer, A.: Model-simulated trend of surface carbon monoxide for the 2001-2010 decade, *Atmos. Chem. Phys.*, 14, 10465-10482, 2014.

Table 1. Measurements of k_1 in He bath-gas

T (K)	p (Torr)	M^a	OH precursor	k_1^b
277	48.6	1.68	H ₂ O ₂	1.59 ± 0.14
292	25.1	0.83	H ₂ O ₂ ^c	0.75 ± 0.07
	50.0	1.65	H ₂ O ₂	1.37 ± 0.08
	75.1	2.47	H ₂ O ₂	1.88 ± 0.12
	102.9	3.39	HNO ₃	2.32 ± 0.15
	206.9	6.81	HNO ₃ ^d	3.73 ± 0.25
	300.7	9.89	HNO ₃	4.64 ± 0.29
	405.8	13.35	HNO ₃	5.54 ± 0.37
	495.6	16.30	HNO ₃	6.29 ± 0.40
	595.0	19.57	HNO ₃	6.83 ± 0.42
	689.1	22.67	HNO ₃	7.46 ± 0.46
	332	28.1	0.82	H ₂ O ₂
56.8		1.65	H ₂ O ₂	0.99 ± 0.08
85.4		2.48	H ₂ O ₂	1.34 ± 0.10

605

^a Molecular density $M(\text{He})$ in units of 10^{18} molecule cm^{-3} . ^b Units of 10^{-12} cm^3 molecule⁻¹ s⁻¹. The errors are 2σ total uncertainty.

^cConcentration range of H₂O₂ $\approx 5\text{-}14 \times 10^{13}$ molecule cm^{-3} . ^dConcentration range of HNO₃ $\approx 5\text{-}9 \times 10^{13}$ molecule cm^{-3} .

Table 2. Measurements of k_1 in N₂-H₂O and He-H₂O bath-gas

610

T / K	$p \text{ (Torr)}$	M^a	$[\text{H}_2\text{O}]^b$	$x_{\text{He}} \text{ OR } x_{\text{N}_2}$	$x_{\text{H}_2\text{O}}$	k_1^c
N ₂ -H ₂ O bath gas						
292	50.2	1.65	0	1	0	2.58 ± 0.16
	50.2	1.66	0.86	0.950	0.050	3.07 ± 0.22
	50.0	1.65	1.62	0.905	0.095	3.45 ± 0.26
	50.0	1.65	2.28	0.866	0.134	3.83 ± 0.26
	50.2	1.66	2.84	0.834	0.166	3.95 ± 0.37
	49.2	1.63	3.27	0.805	0.195	4.10 ± 0.27
	50.0	1.65	4.06	0.754	0.246	4.47 ± 0.18^d
He-H ₂ O bath gas						
277	48.6	1.68	0	1	0	1.59 ± 0.11
	47.6	1.66	0.9	0.946	0.054	2.27 ± 0.15
	48.0	1.67	1.42	0.915	0.085	2.63 ± 0.17
	48.7	1.7	2	0.882	0.118	3.13 ± 0.24
291	50.0	1.65	0	1	0	1.37 ± 0.08
	50.6	1.68	0.64	0.962	0.038	1.99 ± 0.14
	51	1.69	1.30	0.923	0.077	2.39 ± 0.21
	50.7	1.68	2.25	0.863	0.137	2.88 ± 0.24
	49.5	1.64	3.06	0.818	0.182	3.43 ± 0.22
	50.8	1.68	3.12	0.810	0.190	3.44 ± 0.24
	49.7	1.65	3.60	0.783	0.217	3.54 ± 0.23
	50.2	1.66	3.94	0.764	0.236	3.72 ± 0.29
50.5	1.67	4.68	0.721	0.279	4.08 ± 0.27	
332	56.8	1.65	0	1	0	0.99 ± 0.06
	56.3	1.64	0.58	0.964	0.036	1.32 ± 0.08
	56	1.63	1.72	0.895	0.105	1.81 ± 0.16
	56.2	1.63	3.3	0.798	0.202	2.43 ± 0.18
	55.9	1.62	4.33	0.733	0.267	2.88 ± 0.22

Unless otherwise indicated, the measurements were performed using H₂O₂ as OH precursor. The concentration range of H₂O₂ was $5\text{-}18 \times 10^{13}$ molecule cm⁻³ for experiments in He-H₂O bath gas and $9\text{-}14 \times 10^{13}$ molecule cm⁻³ for experiments in N₂-H₂O bath gas. ^a Molecular density M(He-H₂O) or M(N₂-H₂O) in units of 10^{18} molecule cm⁻³. ^b Units of 10^{17} molecule cm⁻³. ^c Units of 10^{-12} cm³ molecule⁻¹ s⁻¹. Errors are 2 σ total uncertainty. ^d measurement performed using O₃-H₂O as OH precursor (with [O₃] = 2×10^{13} molecule cm⁻³).

615

Table 3. Parameters for calculating k_1 using Eqn. (15) and (16)

Bath-gas	k_0^a	T -dependence of k_0 (m , q or o)	k_∞^b	F_c
N ₂	2.6×10^{-30}	3.6 (m)	6.3×10^{-11}	0.39
O ₂	2.0×10^{-30}	3.6 (q)		
H ₂ O	15.9×10^{-30}	3.4 (o)		

620

^a Units of $\text{cm}^6 \text{ molecule}^{-2} \text{ s}^{-1}$. ^b Units of $\text{cm}^3 \text{ molecule}^{-1} \text{ s}^{-1}$. Note that k_∞ is independent of temperature ($n = 0$).

Figure Captions:

625

Figure 1. Values of k_1 from this study (black squares) as a function of He concentration at 292 K. Errors are 2σ statistical only. The solid line is a fit to our data using Eqn. (4) with $k_0 = 1.4 \times 10^{-30} \text{ cm}^6 \text{ molecule}^{-2} \text{ s}^{-1}$, $k_\infty = 6.3 \times 10^{-11} \text{ cm}^3 \text{ molecule}^{-1} \text{ s}^{-1}$, $F_c = 0.32$, $m = 3.1$ and $n = 0$. Previous datasets at room temperature (Wine et al. (1979), D'Ottone et al. (2001), Anastasi and Smith (1976) and Morley and Smith (1972)) are displayed for comparison.

630

Figure 2. Comparison between the present dataset, the high pressure measurements by Hippler et al. (2006) and the low pressure measurements by Anderson et al. (1974), Westenberg and Dehaas (1972), Anderson (1980) and Erler et al. (1977). All measurements were made at room-temperature. The black line is our parameterisation with $k_0 = 1.4 \times 10^{-30} \text{ cm}^6 \text{ molecule}^{-2} \text{ s}^{-1}$, $k_\infty = 6.3 \times 10^{-11} \text{ cm}^3 \text{ molecule}^{-1} \text{ s}^{-1}$, $m = 3.1$, $n = 0$ and $F_c = 0.32$.

635 **Figure 3 a)** Data obtained in $\text{N}_2\text{-H}_2\text{O}$ bath-gas (50 Torr, 292 K). **b)** Data obtained in $\text{He-H}_2\text{O}$ bath-gas (50 Torr, 291 K). Both panels display first-order, OH decay constants in various concentrations of NO_2 and different mole fractions of H_2O . The solid lines represent least squares linear fits to Eqn. (2).

Figure 4. a) k_1 as a function of $x_{\text{H}_2\text{O}}$ at 50 Torr $\text{N}_2\text{-H}_2\text{O}$ and 292 K. The line represents a least squares, multivariate fit (Eqn. 7 and 8) with $k_\infty = 6.3 \times 10^{-11} \text{ cm}^3 \text{ molecule}^{-2} \text{ s}^{-1}$, $k_0^{\text{N}_2} = 2.6 \times 10^{-30} \text{ cm}^6 \text{ molecule}^{-2} \text{ s}^{-1}$, $F_c = 0.39$, $m = 3.6$, $k_0^{\text{H}_2\text{O}} = 15.9 \times 10^{-30} \text{ cm}^6 \text{ molecule}^{-2} \text{ s}^{-1}$, $o = 3.4$. **b)** k_1 as a function of $x_{\text{H}_2\text{O}}$ in $\text{He-H}_2\text{O}$ mixtures at 277, 291 and 332 K. The solid lines represent a least squares, multivariate fit (Eqn. 7 and 9 to 12) where $k_\infty = 6.3 \times 10^{-11} \text{ cm}^3 \text{ molecule}^{-2} \text{ s}^{-1}$, $k_0^{\text{He}} = 1.4 \times 10^{-30} \text{ cm}^6 \text{ molecule}^{-2} \text{ s}^{-1}$, $F_c^{\text{He}} = 0.32$, $m = 3.1$, $k_0^{\text{H}_2\text{O}} = 15.9 \times 10^{-30} \text{ cm}^6 \text{ molecule}^{-2} \text{ s}^{-1}$, $F_c^{\text{H}_2\text{O}} = 0.39$ and $o = 3.4$.

645 **Figure 5.** Annual average effect of H_2O on k_1 expressed as the fractional change in the rate coefficient at the Earth's surface when setting the mole fraction of water vapour to zero in Eqn. 15.

Figure 6 Global values of $\frac{k_1^{\text{IUPAC}}}{k_1^{\text{this work}}}$ (upper panel) and $\frac{k_1^{\text{NASA}}}{k_1^{\text{this work}}}$ (lower panel). k_1 is the overall rate coefficient (both channels) for Reaction R1 calculated using the parameters from this work ($k_1^{\text{this work}}$) and those presently recommended by the IUPAC (k_1^{IUPAC}) and NASA (k_1^{NASA}) data evaluation panels. The black line represents the model tropopause.

Figure 7. Effect of different parameterisations of k_1 on the global (zonal and yearly averaged) HNO_3 to NO_2 ratio. The upper panel plots $\frac{\text{HNO}_3}{\text{NO}_2}(\text{IUPAC})/\frac{\text{HNO}_3}{\text{NO}_2}(\text{this work})$, the lower panel plots $\frac{\text{HNO}_3}{\text{NO}_2}(\text{NASA})/\frac{\text{HNO}_3}{\text{NO}_2}(\text{this work})$. The black line represents the model tropopause.

655

Figure 8. Model (EMAC) ratio of HOONO (formed in the reaction of NO_2 with OH) to HO_2NO_2 (formed in the reaction of NO_2 with HO_2) calculated using the present parameterisation of k_1 and equating the (unknown) rate coefficients for loss of HOONO via reaction with OH or photolysis to those of HO_2NO_2 . The black line represents the model tropopause.

660

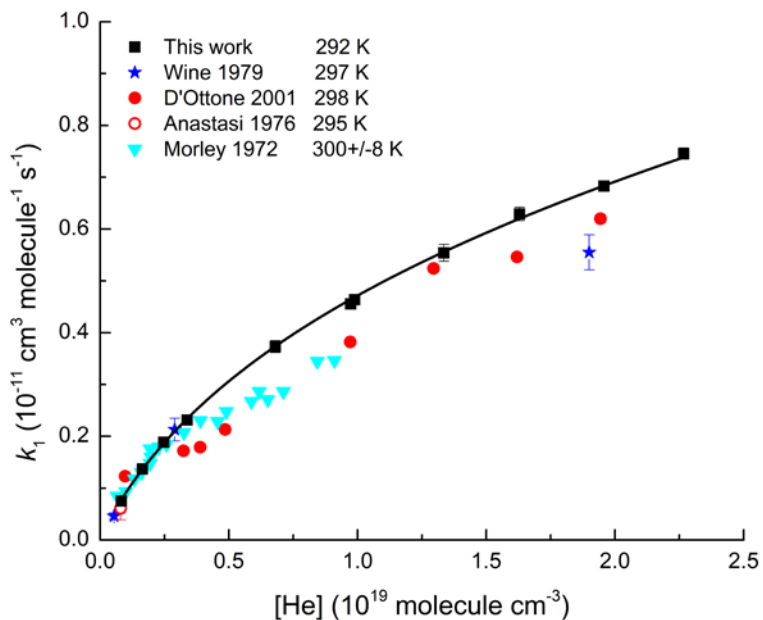


Figure 1. Values of k_1 from this study (black squares) as a function of He concentration at 292 K. Errors are 2σ statistical only. The solid line is a fit to our data using Eqn. (4) with $k_0 = 1.4 \times 10^{-30} \text{ cm}^6 \text{ molecule}^{-2} \text{ s}^{-1}$, $k_\infty = 6.3 \times 10^{-11} \text{ cm}^3 \text{ molecule}^{-1} \text{ s}^{-1}$, $F_c = 0.32$, $m = 3.1$ and $n = 0$. Previous datasets at room temperature (Wine et al. (1979), D'Ottone et al. (2001), Anastasi and Smith (1976) and Morley and Smith (1972)) are displayed for comparison.

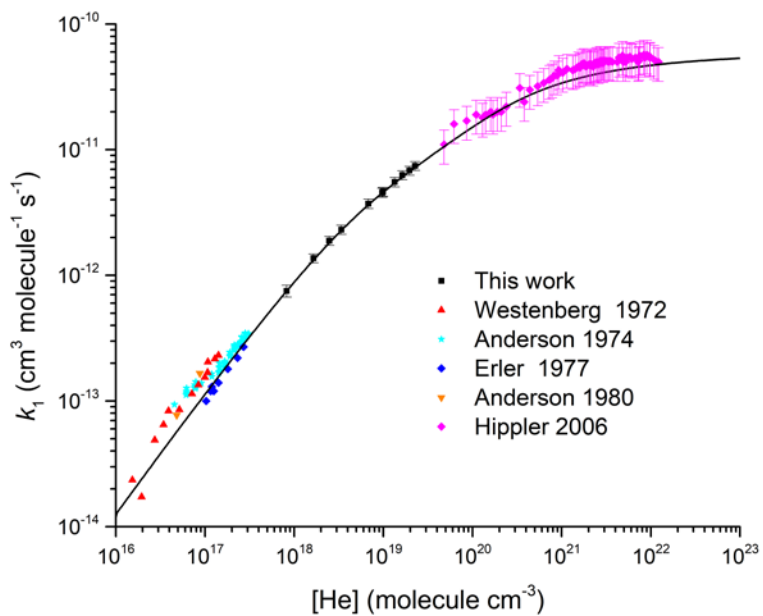


Figure 2. Comparison between the present dataset, the high pressure measurements by Hippler et al. (2006) and the low pressure measurements by Anderson et al. (1974), Westenberg and Dehaas (1972), Anderson (1980) and Erler et al. (1977). All measurements were made at room-temperature. The black line is our parameterisation with $k_0 = 1.4 \times 10^{-30} \text{ cm}^6 \text{ molecule}^{-2} \text{ s}^{-1}$, $k_\infty = 6.3 \times 10^{-11} \text{ cm}^3 \text{ molecule}^{-1} \text{ s}^{-1}$, $m = 3.1$, $n = 0$ and $F_c = 0.32$.

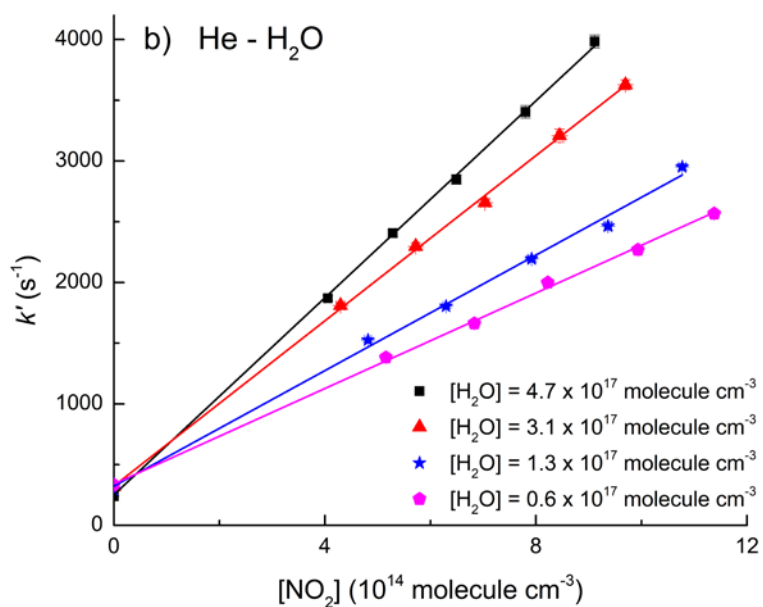
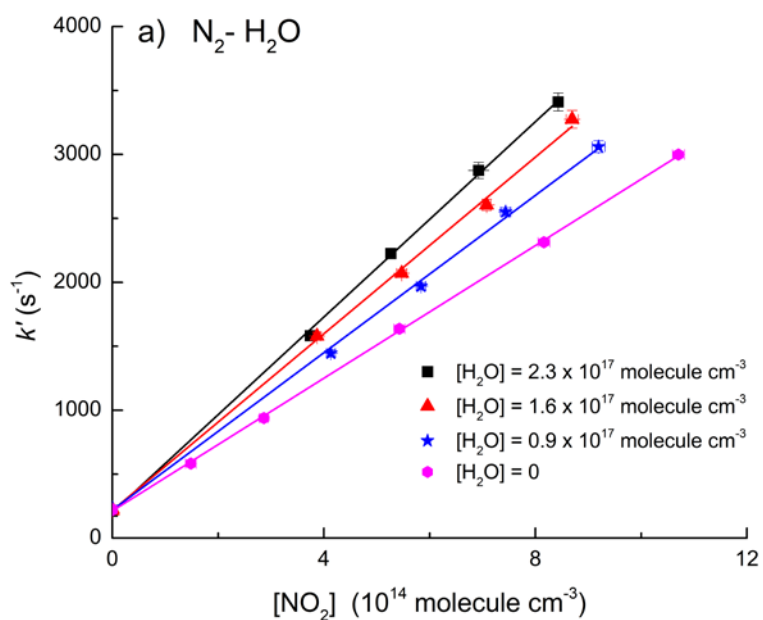


Figure 3 a) Data obtained in $\text{N}_2\text{-H}_2\text{O}$ bath-gas (50 Torr, 292 K). b) Data obtained in $\text{He-H}_2\text{O}$ bath-gas (50 Torr, 291 K). Both panels display first-order, OH decay constants in various concentrations of NO_2 and different mole fractions of H_2O . The solid lines represent least squares linear fits to Eqn. (2).

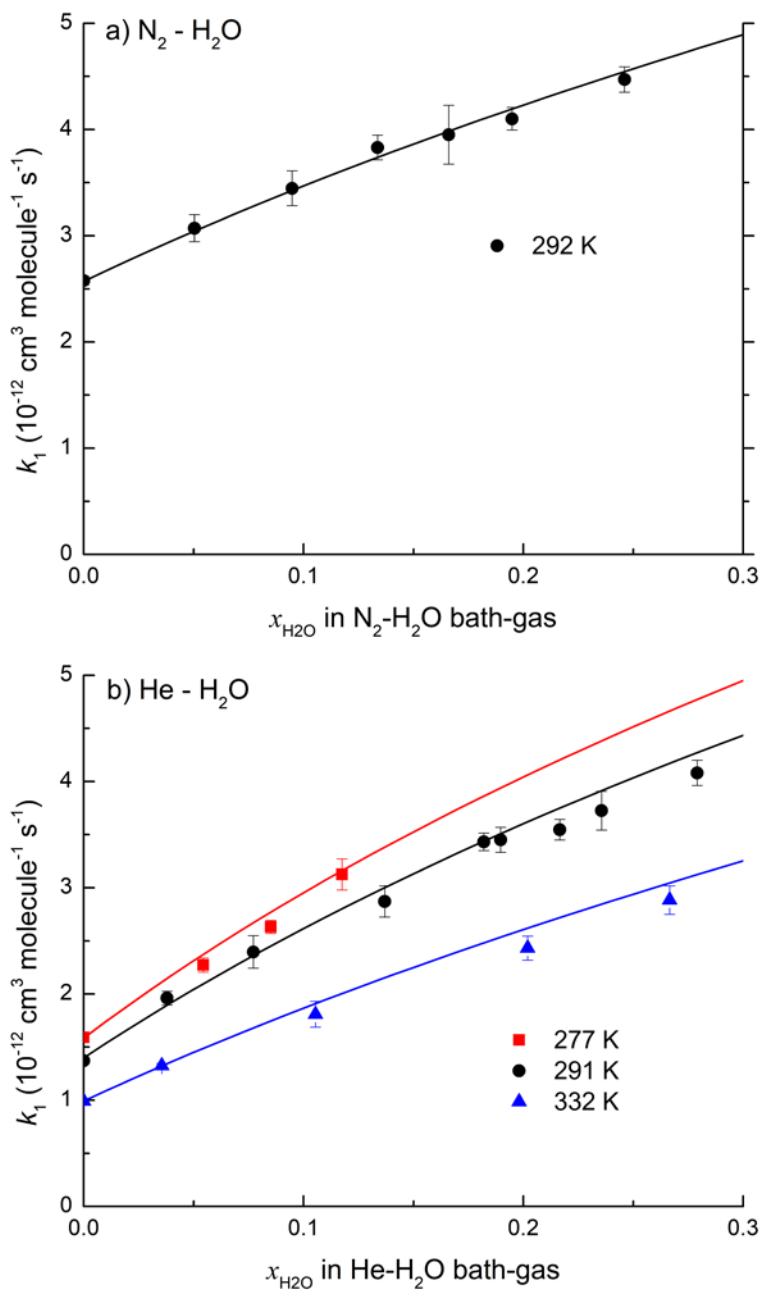


Figure 4. a) k_1 as a function of $x_{\text{H}_2\text{O}}$ at 50 Torr N₂-H₂O and 292 K. The line represents a least squares, multivariate fit (Eqn. 7 and 8) with $k_\infty = 6.3 \times 10^{-11} \text{ cm}^3 \text{ molecule}^{-2} \text{ s}^{-1}$, $k_0^{\text{N}_2} = 2.6 \times 10^{-30} \text{ cm}^6 \text{ molecule}^{-2} \text{ s}^{-1}$, $F_c = 0.39$, $m = 3.6$, $k_0^{\text{H}_2\text{O}} = 15.9 \times 10^{-30} \text{ cm}^6 \text{ molecule}^{-2} \text{ s}^{-1}$, $o = 3.4$. b) k_1 as a function of $x_{\text{H}_2\text{O}}$ in He-H₂O mixtures at 277, 291 and 332 K. The solid lines represent a least squares, multivariate fit (Eqn. 7 and 9 to 12) where $k_\infty = 6.3 \times 10^{-11} \text{ cm}^3 \text{ molecule}^{-2} \text{ s}^{-1}$, $k_0^{\text{He}} = 1.4 \times 10^{-30} \text{ cm}^6 \text{ molecule}^{-2} \text{ s}^{-1}$, $F_c^{\text{He}} = 0.32$, $m = 3.1$, $k_0^{\text{H}_2\text{O}} = 15.9 \times 10^{-30} \text{ cm}^6 \text{ molecule}^{-2} \text{ s}^{-1}$, $F_c^{\text{H}_2\text{O}} = 0.39$ and $o = 3.4$.

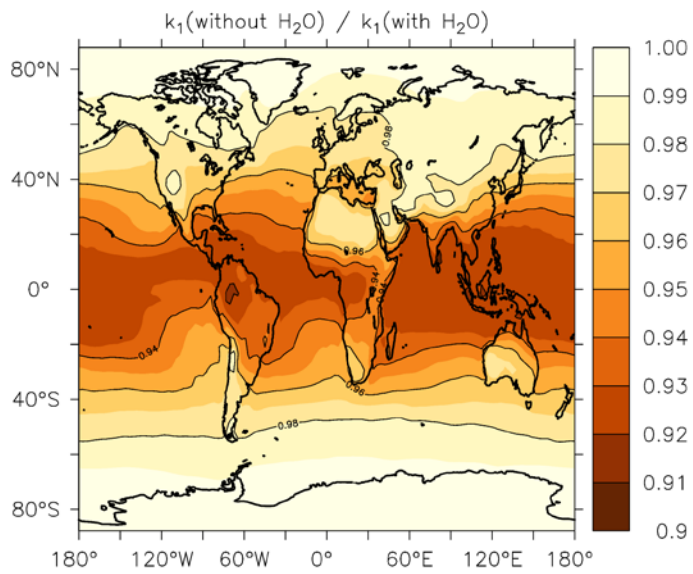


Figure 5. Annual average effect of H₂O on k_1 expressed as the fractional change in the rate coefficient at the Earth's surface when setting the mole fraction of water vapour to zero in Eqn. 15.

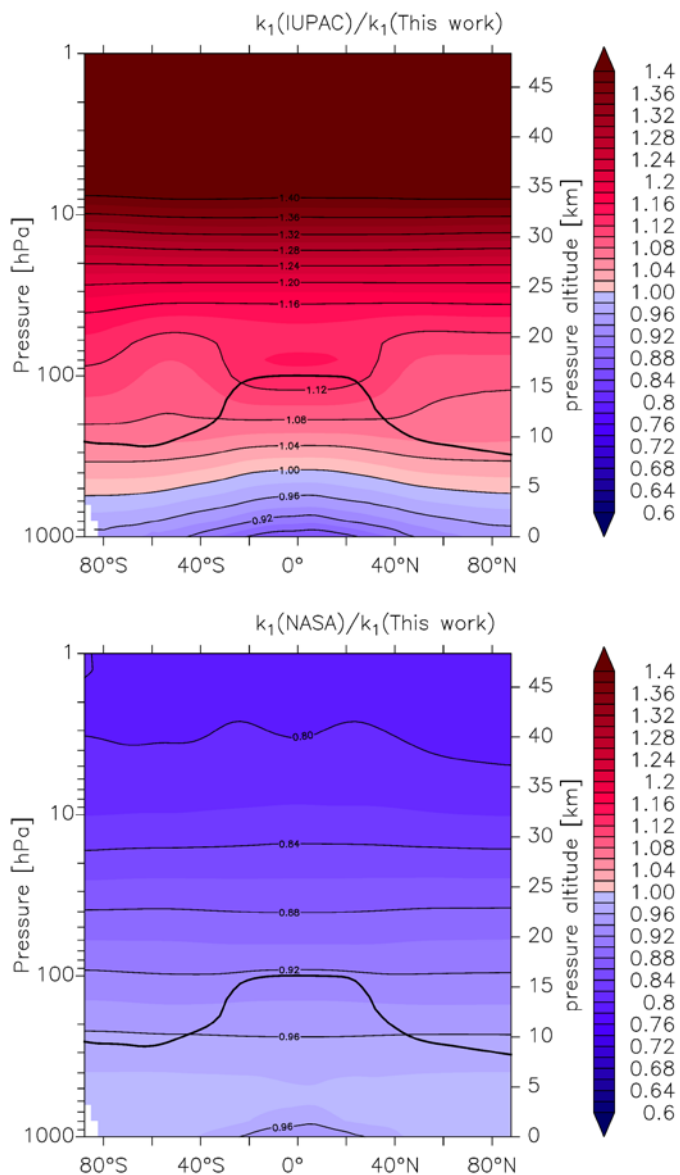


Figure 6 Global values of $\frac{k_1^{\text{IUPAC}}}{k_1^{\text{this work}}}$ (upper panel) and $\frac{k_1^{\text{NASA}}}{k_1^{\text{this work}}}$ lower panel). k_1 is the overall rate coefficient (both channels) for Reaction R1 calculated using the parameters from this work ($k_1^{\text{this work}}$) and those presently recommended by the IUPAC (k_1^{IUPAC}) and NASA (k_1^{NASA}) data evaluation panels. The black line represents the model tropopause.

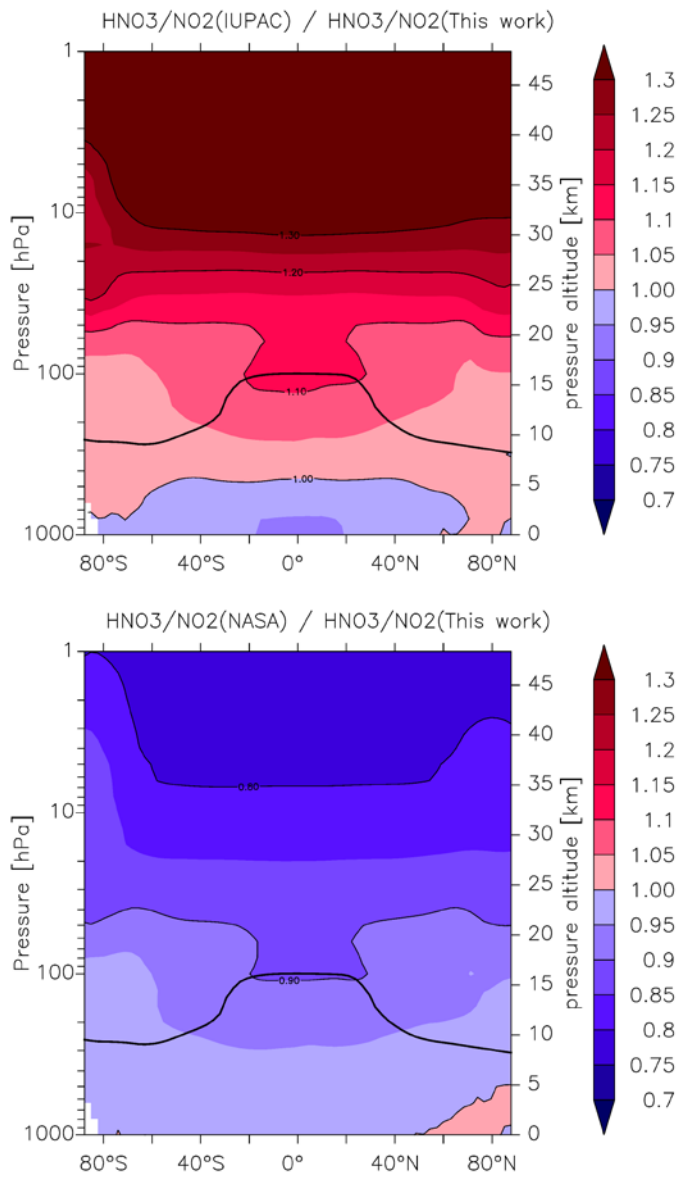


Figure 7. Effect of different parameterisations of k_1 on the global (zonal and yearly averaged) HNO_3 to NO_2 ratio. The upper panel plots $\frac{\text{HNO}_3}{\text{NO}_2}(\text{IUPAC})/\frac{\text{HNO}_3}{\text{NO}_2}(\text{this work})$, the lower panel plots $\frac{\text{HNO}_3}{\text{NO}_2}(\text{NASA})/\frac{\text{HNO}_3}{\text{NO}_2}(\text{this work})$. The black line represents the model tropopause.

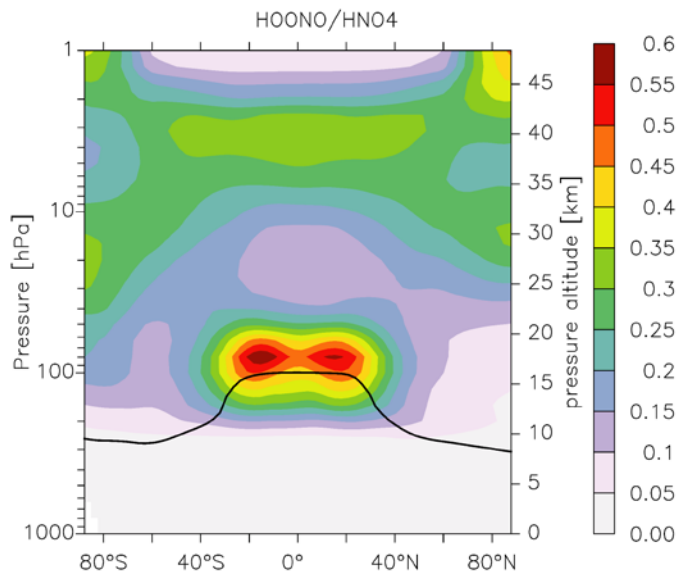


Figure 8. Model (EMAC) ratio of HOONO (formed in the reaction of NO_2 with OH) to HO_2NO_2 (formed in the reaction of NO_2 with HO_2) calculated using the present parameterisation of k_1 and equating the (unknown) rate coefficients for loss of HOONO via reaction with OH or photolysis to those of HO_2NO_2 . The black line represents the model tropopause.